



HAL
open science

Investigating the hydromechanical behaviour of bentonite pellets by swelling pressure tests and discrete element modelling

Benjamin Darde, Jean-Noël Roux, Jean-Michel Pereira, Patrick Dangla, Jean Talandier, Minh Ngoc Vu, Anh Minh A.M. Tang

► To cite this version:

Benjamin Darde, Jean-Noël Roux, Jean-Michel Pereira, Patrick Dangla, Jean Talandier, et al.. Investigating the hydromechanical behaviour of bentonite pellets by swelling pressure tests and discrete element modelling. *Acta Geotechnica*, 2021, 16 (2), pp.507-524. 10.1007/s11440-020-01040-5 . hal-03053589

HAL Id: hal-03053589

<https://enpc.hal.science/hal-03053589v1>

Submitted on 11 Dec 2020

HAL is a multi-disciplinary open access archive for the deposit and dissemination of scientific research documents, whether they are published or not. The documents may come from teaching and research institutions in France or abroad, or from public or private research centers.

L'archive ouverte pluridisciplinaire **HAL**, est destinée au dépôt et à la diffusion de documents scientifiques de niveau recherche, publiés ou non, émanant des établissements d'enseignement et de recherche français ou étrangers, des laboratoires publics ou privés.

TITLE:

Investigating the hydromechanical behaviour of bentonite pellets by swelling pressure tests and discrete element modelling.

AUTHORS:

1) DARDE Benjamin

Affiliation : (1) Navier, Ecole des Ponts, Univ Gustave Eiffel, CNRS, Marne-la-Vallée, France; and (2) French National Radioactive Waste Management Agency (Andra), Châtenay-Malabry, France

Address: Ecole des Ponts ParisTech, Laboratoire Navier, 6-8 avenue Blaise Pascal, 77455 Marne-la-Vallée, France

Email: benjamin.darde@enpc.fr

2) ROUX Jean-Noël

Affiliation: Navier, Ecole des Ponts, Univ Gustave Eiffel, CNRS, Marne-la-Vallée, France

Address: Ecole des Ponts ParisTech, Laboratoire Navier, 2 allée Kepler, 77420 Champs-sur-Marne, France

Email: jean-noel.roux@ifsttar.fr

3) PEREIRA Jean-Michel

Affiliation: Navier, Ecole des Ponts, Univ Gustave Eiffel, CNRS, Marne-la-Vallée, France

Address: Ecole des Ponts ParisTech, Laboratoire Navier, 6-8 avenue Blaise Pascal, 77455 Marne-la-Vallée, France

Email: jean-michel.pereira@enpc.fr

4) DANGLA Patrick

Affiliation: Navier, Ecole des Ponts, Univ Gustave Eiffel, CNRS, Marne-la-Vallée, France

Address: Ecole des Ponts ParisTech, Laboratoire Navier, 6-8 avenue Blaise Pascal, 77455 Marne-la-Vallée, France

Email: patrick.dangla@ifsttar.fr

5) TALANDIER Jean

Affiliation: French National Radioactive Waste Management Agency (Andra), Châtenay-Malabry, France

Address: Andra, DRD/MFS, 1-7 rue Jean Monnet, Parc de la croix blanche, 92298 Châtenay-Malabry, France

Email: jean.talandier@andra.fr

6) VU Minh Ngoc

Affiliation: French National Radioactive Waste Management Agency (Andra), Châtenay-Malabry, France

Address: Andra, DRD/MFS, 1-7 rue Jean Monnet, Parc de la croix blanche, 92298 Châtenay-Malabry, France

Email: minh-ngoc.vu@andra.fr

7) TANG Anh Minh*

Affiliation: Navier, Ecole des Ponts, Univ Gustave Eiffel, CNRS, Marne-la-Vallée, France

Address: Ecole des Ponts ParisTech, Laboratoire Navier, 6-8 avenue Blaise Pascal, 77455 Marne-la-Vallée, France

Email: anh-minh.tang@enpc.fr

*Corresponding author.

ACKNOWLEDGEMENTS

The present work is supported by the French National Radioactive Waste Management Agency (Andra), which is gratefully acknowledged.

ABSTRACT

Bentonite pellet mixtures are candidate material for the sealing of galleries in radioactive waste disposals. The hydromechanical behaviour of assemblies of bentonite pellets is investigated upon partial hydration through (i) suction-controlled swelling pressure tests in the laboratory and (ii) discrete element method (DEM) simulations. The combination of these experimental and numerical approaches highlights that, before the mixture homogenisation, the swelling pressure develops in two phases. The first phase is characterised by an increase of contact forces between pellets. The second phase is characterised by plasticity at contacts between pellets and is controlled by the progressive decrease of pellet strength and stiffness upon hydration. In addition, numerical results highlight that the swelling pressure measured in the laboratory can be influenced by the sample preparation, the cell size, and the diameter of the pressure sensor.

Keywords: Expansive soils; Pellets; Swelling pressure; DEM simulations

1 **1. Introduction**

2
3 Compacted bentonite-based materials are a candidate material for engineered barriers in
4 radioactive waste disposal concepts due to their low permeability, good radionuclide retention
5 capacity and ability to swell upon hydration, resulting in the filling of technological voids and a
6 swelling pressure development on the tunnel walls. The development of a swelling pressure
7 contributes to the decrease of hydraulic conductivity in the excavation induced damaged zone.
8 In this respect, the hydromechanical behaviour of compacted bentonite materials has been
9 widely studied over the last two decades [1-16].

10
11 The use of pellet-based bentonite materials has been considered an interesting solution for the
12 installation of engineered barriers because of operational convenience [17-27]. Pellet materials
13 are laid as a dry granular assembly in the galleries and subsequently undergo swelling upon
14 hydration from the host rock pore water. Upon hydration, pellet materials are known to lose their
15 initial granular structure and reach a homogeneous final state [18, 19, 27]. Like other bentonite
16 materials, the final swelling pressure developed by pellet materials in constant volume
17 conditions can be estimated from their initial dry density [28, 29].

18
19 Before homogenisation, the hydromechanical behaviour of pellet materials is still not perfectly
20 understood. Upon pellet swelling, the swelling pressure is influenced by the granular nature of
21 the material [28, 29]. Interactions at contacts between pellets and stiffness decrease of the
22 pellets during hydration are thought to control the overall hydromechanical behaviour [31].

23
24 It is proposed in the present study to evaluate the influence of interactions at contacts on the
25 macroscopic response of bentonite pellet assemblies upon hydration. The objective is to obtain
26 an insight into the hydromechanical behaviour of pellet materials upon hydration, before
27 reaching a homogeneous state. In this purpose, swelling pressure tests are performed in the
28 laboratory on pellet materials. Discrete Element Method (DEM) is then used to model the
29 swelling pressure tests.

30

31 In DEM simulations [32], each grain is modelled individually. DEM allows to study the influence
32 of the behaviour of one pellet and interactions at contacts between pellets on the behaviour of
33 the granular assembly. DEM has been successfully used in similar engineering problems
34 involving irreversible changes in the volume of grains, such as the effect of particle thermal
35 expansion in granular materials [33, 34]; or grain-scale modelling of the swelling behaviour of
36 absorbent polymer particles upon hydration in hygienic products [35].

37

38 The ability of DEM to access grain-scale phenomena can provide valuable information about
39 the behaviour of assemblies of pellets upon hydration-induced pellet swelling. These latter can
40 be obtained neither through experimental tests, since only macroscopic phenomena are
41 measurable most of the time, nor through finite element method (FEM) simulations, which
42 require a homogeneous continuum. In the present study, DEM is an interesting tool to study the
43 hydromechanical behaviour of pellet materials before homogenisation while providing a better
44 understanding of the results of laboratory tests.

45

46 The present paper applies DEM to the simulation of the partial hydration of expansive clay pellet
47 assemblies. In DEM, the behaviour of each pellet is based on the hydromechanical model for a
48 single pellet proposed by Darde et al. (2018) [36]. Interactions between pellets are described by
49 contact mechanics and characterised by the Hertz law and the Coulomb friction [37]. Some
50 preliminary results obtained using this approach can be found in Darde et al. (2020) [38]. In the
51 present work, more comprehensive description, analysis and discussion of the experimental
52 study and numerical simulations are presented. The modelling approach is validated by
53 simulating suction-controlled swelling pressure tests carried out at laboratory scale.

54

55 Materials and experimental methods regarding the swelling pressure tests are first described.
56 The main features of the DEM simulations are presented in the second part. Both experimental
57 and numerical results are then presented and discussed in the third and fourth parts,
58 respectively. Important contributions and main perspectives arising from the present study then
59 constitute the paper conclusion.

60

61 **2. Material and Experimental methods**

62

63 **2.1. Bentonite pellets**

64

65 The material studied in the framework of the present study is an assembly of MX80 bentonite
66 granules or pellets. MX80 is a sodium (Na)-bentonite from Wyoming (USA). Its main properties
67 are summarised in Table 1.

68

69 Pellets are obtained from MX80 bentonite powder by pressure casting (compaction in a mould).

70 Granules are composed of a central cylinder with spherical caps at both ends. Their initial dry
71 density, suction value and water content are 1.90 g/cm^3 , 89 MPa and 0.122, respectively [36].

72 The main initial properties of the pellets are listed in Figure 1 and Table 2.

73

74 **2.2. Constant-volume swelling pressure tests**

75

76 2.2.1. Pellet assembly

77

78 In the French concept of radioactive waste disposal, a bentonite pellet and powder (crushed
79 pellets) mixture is candidate material for the sealing plugs preventing fluid migrations. The dry
80 density of the reference mixture and the dry mass proportion of pellets and powder are 1.50
81 g/cm^3 and 70/30, respectively. The mixture is laid in a dry state as a granular assembly.

82 Interactions between high-density granules are thought to have an influence on the material
83 mechanical behaviour at the beginning of hydration, especially at the structure scale if
84 heterogeneity of powder content arises [22], as a consequence of either an imperfect laying or
85 particle segregation.

86

87 In the present work, the influence of the granular structure of the material on the macroscopic
88 response at the beginning of hydration is studied through constant-volume swelling pressure
89 tests carried out on a pellet assembly without powder. The material dry density in the present
90 study is thus 1.05 g/cm^3 . The initial pellet volume fraction is 0.553.

91

92 2.2.2. Isochoric cell

93

94 The swelling pressure in the present study is defined as the pressure developed by the material
95 against the upper wall of a cylindrical isochoric cell upon hydration. A pressure sensor (BER-A-
96 5MP15S from Kyowa, capacity of 5 MPa) at the centre of the cell upper wall measures the
97 swelling pressure as a function of elapsed time.

98 The cylinder dimensions are given in Table 3. A sketch of the cell is presented in Figure 2.

99

100 2.2.3. Sample preparation

101

102 Two samples are prepared (referred to as SP1 and SP2 in the following). In both cases, the
103 target dry density (1.05 g/cm^3) is reached by introducing a mass of pellets of 99.9 g. This mass
104 corresponds to 209 pellets. The 209 pellets are placed one by one in the cell in successive
105 layers [22]. Cells are then closed by placing the upper wall so that the cell height is 30 mm. The
106 closure step can induce a pressure increase if upper wall-pellet contacts are created. The
107 preparation step of SP1 and SP2 resulted in an initial pressure of 10 kPa and 55 kPa after the
108 cell closure, respectively.

109

110 2.2.4. Suction-controlled hydration at constant room temperature

111

112 Hydration is performed step by step through the vapour equilibrium technique as described in
113 [2, 19, 39]. Suction is decreased from 89 MPa (initial state) to 4 MPa (SP1 test) and 9 MPa
114 (SP2 test). Salt solutions used in the study are listed in Table 4 along with their corresponding
115 suction values.

116

117 A peristaltic pump makes air circulate through the salt solution to impose a constant target
118 relative humidity, then through the isochoric cell. Humid air is allowed to circulate directly from
119 the bottom to the top of the cell through a side tube. Thus, no excessive air pressure is

120 developed when using the peristaltic pump and humid air is considered to circulate freely inside
121 the inter-pellet porosity (Figure 3). Room temperature is $20^{\circ}\text{C} \pm 1^{\circ}\text{C}$.

122

123 As humid air circulates in the isochoric cell, pellets are hydrated and swell. Pellet swelling in an
124 isochoric cell results in the development of a swelling pressure which is measured by the
125 pressure sensor at the centre of the top wall.

126

127 Equilibrium is considered to be reached when the pressure measured by the sensor remains
128 constant for a minimum of 3 days. The final pressure value is used to draw the suction-swelling
129 pressure relationship. The current salt solution is then replaced by the following one (Table 4) to
130 impose the next relative humidity step.

131

132

133 **3. Discrete Element Method simulations of the swelling pressure tests**

134

135 **3.1. Overview of the method**

136

137 DEM simulations are carried out by using an in-house program [40]. In the DEM simulations
138 carried out, each pellet is modelled as a sphere. A molecular dynamics scheme in the
139 quasistatic limit is used [40]. The hydromechanical behaviour of each pellet upon hydration is
140 described by the model proposed by [36] for a single pellet.

141

142 The sphere diameter a_{eq} is chosen such that its volume coincides with the pellet volume V :

143

$$(1) \quad a_{eq} = \left(\frac{6V}{\pi} \right)^{1/3}$$

144

145 The initial value of a_{eq} is obtained from initial values of mass and density: $a_{eq,0} = 7.53 \text{ mm}$.

146

147 In order to assess the ability of the model to reproduce the hydromechanical behaviour of the
148 granular assembly, swelling pressure tests are simulated. In the simulations, the isochoric cell is

149 modelled as a rigid cylinder (infinite Young's modulus), the height and diameter of which are the
150 same as the cell used for the swelling pressure tests. 209 pellets are simulated in each
151 simulations, corresponding to the number of granules in the swelling pressure tests performed
152 in the laboratory, thus the same pellet volume fraction.

153

154 Simulations are carried out in two main steps:

- 155 - the preparation step, corresponding to the installation of model beads inside the
156 cylinder and the cell closure;
- 157 - the hydration steps.

158

159 Three different types of simulations are carried out and referred to as DEM1; DEM2; DEM3. For
160 each type, 100 calculations are performed to quantify the variability of the results. The
161 difference between the simulations is the initial position of the beads following the sample
162 preparation. This point is described in a dedicated section. DEM1 simulations aim at
163 reproducing the swelling pressure tests with optimised preparation to avoid initial pressure (no
164 friction during preparation). DEM2 simulations aim at assessing the influence of a less
165 optimised initial state following the preparation step on the material behaviour upon hydration
166 (friction during preparation). In both DEM1 and DEM2, contact friction is taken into account
167 during hydration. In DEM3 simulations, no contact friction is taken into account during both
168 preparation and hydration steps (Table 5).

169

170 The following parts provide details concerning the model for a pellet, contact laws, hydration
171 and preparation steps.

172

173 **3.2. Hydromechanical behaviour of a pellet**

174

175 From grain-level experimental characterisation, Darde et al. (2018) [36] proposed a model
176 describing the evolution of pellet stiffness, volumetric strain and strength upon suction decrease
177 (Figures 4a and 4b). Pellets are characterised by their microstructure, assumed to be fully-
178 saturated. The following notations are used for the model parameters:

- 179 - E_m is the pellet Young modulus;
- 180 - ν is the pellet Poisson ratio, taken equal to 0.3;
- 181 - ε_{vm} is the volumetric strain;
- 182 - s_0 is the initial pellet suction;
- 183 - R_A is the strength;
- 184 - α_m ; β_m and C_A are model parameters, respectively taken equal to 0.024 MPa^{-1} ; 0.016
- 185 MPa^{-1} and 0.12 N/MPa [36];
- 186 - p' is the effective mean stress. Since pellets are considered fully-saturated, p' is taken
- 187 equal to the sum of the total mean stress p and the suction s . In the considered suction
- 188 range, $s \gg p$ and it is assumed that $p' = s$.

189 Using these notations, the model equations describing the pellet behaviour are:

190

$$(2) \quad E_m(p') = 3(1 - 2\nu) \frac{1}{\beta_m} \exp(\alpha_m p')$$

$$(3) \quad \varepsilon_{vm}(p') = \frac{\beta_m}{\alpha_m} [\exp(-\alpha_m s_0) - \exp(-\alpha_m p')]$$

$$(4) \quad R_A(p') = C_A E_m(p')$$

$$(5) \quad p' = p + s = s$$

191

192 The above equations are used in DEM to determine the mechanical properties of each particle
193 at any value of suction.

194

195

196 3.3. Hydration modelling

197

198 Pellet hydration and subsequent swelling are simulated by a simultaneous increase of all the
199 bead diameters. It is therefore assumed that all pellets get hydrated at the same rate. The
200 diameter increase at each hydration step i varies from 0.1 % to 0.9 % from initial state (89 MPa

201 of suction) to final state (9 MPa of suction). 60 diameter increments are imposed, for an overall
 202 diameter increase of ~15 %:

203

$$(6) \quad a_{eq\ i+1} = \lambda_i a_{eq\ i}$$

204

205 Where:

206

$$(7) \quad \lambda_i = \exp \left[\ln \left(\frac{\lambda_f}{\lambda_0} \right) \left(\frac{a_{eq\ i} - a_{eq\ 0}}{a_{eq\ f} - a_{eq\ 0}} \right) + \ln(\lambda_0) \right]$$

207

208 Where λ_i characterises the diameter increment; λ_f and λ_0 are parameters taken equal to 10^{-2} and
 209 10^{-3} , respectively; $a_{eq\ i}$ and $a_{eq\ f}$ are the equivalent diameters at step i and at the final suction
 210 value, respectively.

211

212 From radius increments, the volume variation is obtained. The suction value corresponding to
 213 each hydration stage is obtained from equation (3). Stiffness and strength are obtained from
 214 equations (2) and (4), respectively.

215

216 Contact laws then allow the granular assembly evolution to be computed, taking into account
 217 the suction-dependency of the aforementioned material parameters.

218

219 **3.4. Contact laws**

220

221 In contacts between two granules of same radius and modulus, the Hertz law (Figure 5) relates
 222 the normal contact elastic force F_N to the normal elastic deflection at contact δ_N^e as:

223

$$(8) \quad F_N = \frac{1}{3} \frac{E_m}{1 - \nu^2} a_{eq}^{1/2} \delta_N^e{}^{3/2}$$

224

225 Contacts between a granule and the infinitely stiff flat walls satisfy:

226

$$(9) \quad F_N = \frac{2^{3/2}}{3} \frac{E_m}{1 - \nu^2} a_{eq}^{1/2} \delta_N^e{}^{3/2}$$

227

228 Granule strength is taken into account by considering perfect plasticity at contacts. The elastic
229 part is described by the Hertz law (equations (8) and (9)) and the elastic limit is given by
230 equation (4). Thus,

231

$$(10) \quad F_N \leq R_A$$

232

233 and plastic deflection can arise for $F_N = R_A$ (Figure 6a).

234

235 Tangential elasticity at contacts is described by a simplified form of the Cattaneo-Mindlin-
236 Deresiewicz laws [37], with due care for energetic consistency and objectivity, as proposed by
237 Agnolin and Roux (2007) [40]. $\dot{\mathbf{F}}_T$, the increment of tangential reaction vector \mathbf{F}_T , is related to
238 $\dot{\boldsymbol{\delta}}_T$, the increment of relative tangential displacement vector $\boldsymbol{\delta}_T$, using the following equation:

239

$$(11) \quad \dot{\mathbf{F}}_T = \frac{2 - 2\nu}{2 - \nu} \frac{dF_N}{d\delta_N} \dot{\boldsymbol{\delta}}_T$$

240

241 The Coulomb condition is checked so that

242

$$(12) \quad F_T \leq \mu F_N$$

243

244 where F_T is the norm of the \mathbf{F}_T vector and μ is a friction coefficient.

245 Sliding can arise for $F_T = \mu F_N$ (Figure 6b). The same value of μ is taken for both pellet-pellet
246 and pellet-wall contacts.

247

248 Damping is taken into account by adding a viscous component to the hertzian elastic force. The
249 viscous force, N^v , in a contact between two pellets is written as:

250

$$(13) \quad N^v = \alpha_v \left(2 m_p \frac{dF_N}{d\delta_N} \right)^{1/2} \frac{d\delta_N}{dt}$$

251

252 Where α_v is a fraction of the critical damping coefficient and m_p is the mass of the pellet. α_v is
253 taken equal to 0.9. Further discussion concerning the damping in contacts can be found in [40].

254

255 **3.5. Numerical sample preparation**

256

257 Numerical samples are prepared by placing pellets one by one in a rigid cylinder. The initial
258 height of the cylinder, $H_{cell\ 0}$, is set at a value of $H_{cell} + a_{eq\ 0}$, where H_{cell} is the cylinder height
259 during the swelling step. This initial value ensures that all the pellets can be placed in the
260 cylinder. A pellet is placed in the cell each second. The first 20 pellets are randomly placed at
261 the bottom of the cell. Then, each bead is placed at a position corresponding to the lowest
262 elevation in the cell to reproduce experimental preparation (Figure 7a). During this process, the
263 granular assembly is constantly being equilibrated under gravity. When all the pellets are placed
264 in the cell, calculation continues until equilibrium of forces and moments is reached. The cell
265 closure is then simulated by incrementally decreasing the cylinder height from $H_{cell\ 0}$ to H_{cell} .
266 Each height decrease is followed by the calculation of a new equilibrium under gravity before a
267 new decrease. The initial solid fraction of all the numerical samples is the same as in
268 experiment (0.553, corresponding to an inter-pellet porosity of 0.447).

269

270 **3.6. Equilibrium of forces and moments**

271

272 At each calculation step, i.e. height decrease during preparation or new suction value during
273 hydration, the granular assembly is considered at equilibrium if both the ratio of the net force
274 F_{net} to the maximum normal force F_{max} and the ratio of the net moment Γ_{net} to the maximum
275 moment Γ_{max} ratio are, on each bead, below a tolerance value ϵ :

276

$$(14) \quad |F_{net}| \leq \epsilon |F_{max}|$$

277

$$(15) \quad |\Gamma_{net}| \leq \epsilon |F_{max}| \frac{a_{eq}}{2}$$

278

279 ϵ is taken equal to 10^{-4} in all the simulations.

280

281 **3.7. Swelling pressure calculation**

282

283 At equilibrium, the swelling pressure P_s^* is computed as the total normal force exerted by the
284 material onto the sensor, divided by the sensor area (Figure 7b). The sensor area is at the
285 centre of the upper wall and defined by the sensor diameter D_{sensor} . Different values of swelling
286 pressure can be calculated from one simulation, depending on the value of D_{sensor} .

287

288 **4. Results**

289

290 **4.1. Experimental suction-swelling pressure relationship**

291

292 The evolution of the swelling pressure is measured as a function of elapsed time. Following a
293 change of imposed suction value, the pressure increases or decreases, then reaches a plateau.
294 For each suction value, the plateau value is retained as the corresponding swelling pressure. A
295 new suction value is then imposed (Figure 8a and 8b). Some pressure fluctuations are
296 measured, and are thought to be related to experimental conditions. Room temperature and
297 humidity variations, slight voltage variations in the measurement apparatus, or opening of the
298 bottle containing salt solutions for cleaning (thus temporary modifying the imposed suction), are
299 examples of external perturbations which influence the measurements. Regular cleaning of the
300 bottle was actually compulsory as salt crystallisation on the bottle side would increase the
301 suction, and salt crystallisation inside the tube plunged in the solution would prevent air
302 circulation.

303

304 Following the cell closure, SP1 initial pressure was 10 kPa at initial suction 89 MPa. Equilibrium
305 then required ~30; ~120; ~75; ~80; ~35 and ~55 days on imposing 82; 59; 38; 25; 9 and 4 MPa,
306 respectively. Following the cell closure, SP2 initial pressure was 55 kPa. Equilibrium in this test
307 required less time, as an overall plateau value was reached at higher suction, resulting in little
308 pressure variations on imposing new suction values. On imposing 82; 59; 40; 38; 25; 13 and 9
309 MPa, equilibrium required ~30; ~10; ~20; ~20; ~15; ~25 and ~30 days to be reached,
310 respectively.

311

312 The suction-swelling pressure relationships obtained for SP1 and SP2 samples are presented in
313 Figure 9. Results highlighted that upon hydration under constant-volume conditions, the
314 swelling pressure of pellet materials increased in two phases within the considered suction
315 range. The first phase is characterised by an increase of swelling pressure. The second phase
316 is characterised by either a plateau or a decrease of swelling pressure. In SP1 test, the axial
317 pressure ($P_{S,XP}$) increases from 10 kPa (closure pressure) to 130 kPa when suction is
318 decreased from 89 MPa (initial state) to 25 MPa. $P_{S,XP}$ slightly increases from 130 kPa to 150
319 kPa when suction is decreased from 25 MPa to 9 MPa, then slightly decreases to 137 kPa
320 when suction is decreased to 4 MPa. In SP2 test, $P_{S,XP}$ increases from 55 kPa (closure
321 pressure) to 180 kPa when suction is decreased from 89 MPa to 25 MPa. After this phase, $P_{S,XP}$
322 decreases from 180 to 130 kPa when suction is decreased from 25 MPa to 9 MPa.

323

324 **4.2. Dismantling of experimental samples**

325

326 SP1 and SP2 isochoric cells were opened after reaching equilibrium at 4 MPa and 9 MPa of
327 suction, respectively. Both SP1 and SP2 samples appeared to be granular. Pellets and
328 macropores could easily be identified (Figure 10a and 10b). Some pellets in contact with the
329 upper wall were deformed in both samples. It was not possible to determine whether it occurred
330 during the closure or during swelling.

331

332 **4.3. Numerical suction-swelling pressure relationship**

333

334 Figure 11 presents the results of swelling pressure as a function of suction obtained in
335 simulations DEM1; DEM2 and DEM3. As a reminder, 100 simulations were carried out for
336 DEM1, DEM2, and DEM3. Only the mean values of swelling pressure are plotted, for a ratio of
337 sensor diameter to initial pellet diameter of 4 (as in experimental tests).

338

339 In DEM1, the mean value of swelling pressure increases from 0 to 330 kPa as suction
340 decreases from 89 MPa to 60 MPa, then slowly decreases to reach 110 kPa at 4 MPa of
341 suction. In DEM2, swelling pressure reaches 500 kPa during the closure step, then slowly
342 decreases to reach 110 kPa at 4 MPa of suction. In DEM3, the pressure slowly increases to 10
343 kPa from 89 MPa to 80 MPa of suction, then increases to 250 kPa at 60 MPa of suction, then
344 slowly decreases to 110 kPa as suction decreases to 4 MPa.

345

346 **4.4. Grain-scale features of numerical samples**

347

348 4.4.1. Contact plasticity

349

350 The evolution of the number of plastic contacts upon hydration is determined in numerical
351 samples. Figures 11a, 11b and 11c present the evolution of the mean plastic contacts
352 proportion for the whole sample, x_c^p , and for contacts between pellets and the upper wall,
353 where pressure is measured, $x_{c\ sup}^p$, for simulations DEM1, DEM2 and DEM3. Results are
354 presented along with the swelling pressure development upon suction decrease. In all samples,
355 the increase in $x_{c\ sup}^p$ is more significant than the increase in x_c^p .

356

357 In DEM1, from initial state to 70 MPa of suction, the swelling pressure increases while no
358 contact has reached the elastic limit. The number of plastic contacts increases sharply between
359 70 MPa and 60 MPa of suction. This suction range corresponds to the peak swelling pressure.
360 The swelling pressure then slowly decreases, as $x_{c\ sup}^p$ reaches a maximum and keeps slowly
361 increasing in the whole sample.

362

363 The evolution of plastic contacts in DEM3 exhibited a similar trend as in DEM1, but the increase
364 of $x_{c\ tot}^p$ and $x_{c\ sup}^p$ was not as sharp as in DEM1. In DEM2, the pressure increase due to the cell
365 closure induced contact plasticity. The influence of the closure step in this case is significant. 25
366 “pellet-upper wall” contacts were created during this step. 15 of these contacts reached the
367 elastic limit during the process, which represents 2.5 % of the overall 600 contacts in the
368 samples. Yet, no significant increase of swelling pressure is recorded upon hydration. The
369 measured pressure keeps decreasing as $x_{c\ tot}^p$ and $x_{c\ sup}^p$ increase.

370

371 4.4.2. Inter-pellet porosity

372

373 At initial state, the porosity was ~0.447. Upon pellet swelling, porosity in DEM progressively
374 decreases and reaches a value slightly below 0.2 (Figure 12). This latter is below the minimal
375 value for a dense packing of spheres of same diameter. It highlights that total deflection at
376 contact is non-negligible at low suction. Considering plasticity in contacts allows the elastic
377 deflection, used in equations (8) and (9), to remain small and avoids reaching unrealistically
378 high contact forces.

379

380 4.4.3. Coordination number

381

382 The coordination number Z , defined by the average number of force-carrying contact per grain,
383 relates to the number of particles N_p , the number of particle-particle contacts $N_{c\ 1}$ and the
384 number of particle-wall contacts $N_{c\ 2}$ as:

385

$$(16) \quad Z = \frac{2 N_{c\ 1} + N_{c\ 2}}{N_p}$$

386

387 Z is calculated following preparation and upon hydration. Results are presented in Figure 12 for
388 DEM1, DEM2 and DEM3 along with the evolution of inter-pellet porosity.

389

390 After closure, the mean coordination number in samples prepared under zero-friction conditions
391 (DEM1 and DEM3) is 5.4. The mean number of contacts in this case is 635, slightly higher than
392 $3 N_p$ [41], as it should be for frictionless beads approaching the limit of small deflections.

393

394 The presence of friction in the assembling stage reduces the number of contacts [40]. Thus
395 samples DEM2 contain 600 contacts on average, with a coordination number of 5.1.

396

397 Upon hydration, the coordination number of frictionless samples (DEM3) increases to a final
398 value of 8.2 (net increase: + 2.8). The coordination number of both DEM1 and DEM2 samples
399 increased at the same rate, reaching final values of 7.5 and 7.2 respectively (net increase: +
400 2.1).

401

402 4.4.4. Variability of the results

403

404 The coefficient of variation (standard deviation to mean value ratio) of swelling pressure,
405 proportion of plastic contacts and coordination number for the three simulation types is
406 calculated from 100 simulations and presented in Figure 13.

407

408 The result variability for swelling pressure and proportion of plastic contacts decreased upon
409 hydration for the three types of simulation. At 9 MPa of suction, its value for swelling pressure
410 reached ~0.10-0.15 (for $D_{sensor} / a_{eq} = 4$). Its value for proportion of plastic contacts reached
411 ~0.03-0.04. The coefficient of variation of coordination number remained low (< 0.02) for the
412 three types of simulation upon hydration.

413

414 **4.5. Influence of the sensor diameter**

415

416 In DEM1, the calculation of swelling pressure from contact forces between pellets and the upper
417 wall is carried out for different values of D_{sensor} . Different suction-swelling pressure relationships
418 are thus obtained. Figure 14 presents the variability of the measured swelling pressure in the
419 100 DEM1 simulations performed, for two values of the $D_{sensor} / a_{eq 0}$ ratio. In both cases, an

420 interval from $m - 2\sigma$ to $m + 2\sigma$ is plotted, with m and σ the mean value and the standard
421 deviation of the swelling pressure, respectively. The mean values are very close for both sensor
422 diameters and are not plotted in Figure 14. The standard deviation significantly increases with
423 decreasing sensor diameter.

424

425 The coefficient of variation is determined for six sensor diameter to pellet diameter ratios, at
426 peak measured pressure and at 9 MPa of suction. Results are plotted in Figure 15. The
427 coefficient of variation of the measured swelling pressure reaches 0.8 to 1.3 in the case where
428 both the sensor diameter and the initial pellet diameter are identical.

429

430

431 **5. Discussion**

432

433 The hydromechanical behaviour of expansive clay pellet materials has been studied through
434 swelling pressure tests at laboratory scale and DEM, providing access to grain-scale
435 phenomena. In the following parts, the model validity is first discussed. Then, the material
436 behaviour upon hydration in constant volume conditions as well as interesting contributions of
437 the DEM to interpretation of laboratory tests results and constitutive modelling using double
438 structure models are discussed.

439

440 **5.1. Model validity**

441

442 The validity of the modelling approach mainly depends on the following assumptions:

- 443 - the material remains granular upon suction decrease;
- 444 - the shape of the simulated beads does not induce significant difference of behaviour;
- 445 - the contact laws are valid;
- 446 - pellet hydration can be simulated by a radius increase.

447

448 Sample dismantling allowed the material granular nature to be observed upon hydration to
449 suction value as low as 4 MPa (Figure 10a and 10b). Furthermore, the shape of the pellets was

450 not notably modified. Only local deformation is observable at contact area. These deformations
451 are irreversible.

452

453 In the simulations, granules are modelled as isotropic spheres. Their real shape is shown to
454 remain nearly identical upon hydration (Figure 10a and 10b), but is characterised by a cylinder-
455 shaped part between two spherical ends (Figure 1 a and 1 b). Pellets are nonetheless
456 characterised by an aspect ratio (total height to diameter ratio) equal to 1 and considered
457 subspherical. Wiacek et al. (2012) [42] showed that uniaxial compression of subspherical pea
458 seeds could effectively be modelled by spheres in DEM. Furthermore, [36] show small
459 differences between axial and radial values of elastic modulus for pellets within the investigated
460 suction range. It is thus thought that isotropic beads are a suitable choice to model these
461 bentonite pellets.

462

463 Assuming linear elasticity, the normal force-deflection relationship at contact is described by the
464 Hertz law (equations (8) and (9)) which had been shown to satisfactorily reproduce the
465 experimental pellet force-deflection relationship [36]. It is proposed to include the influence of
466 grain failure in the model to avoid reaching unrealistically high normal force values. It is
467 assumed that failure initiates at contact and does not depend on the grain stress state. The
468 pellet strength in the granular assembly is thus assumed to be described by the empirical
469 equation proposed for free swelling conditions (equation (4)). As suggested by Figure 10a and
470 10b, particle failure is more characterised by an irreversible deformation at contact or apparition
471 of cracks than by a general crushing. In this respect, contact plasticity is thought to be an
472 interesting way of modelling this phenomenon as it allows irreversible deflection to arise in
473 simulations. Elastic-plastic contact modelling approach [43, 44] is thus preferred to grain
474 crushing modelling approach [45, 46] to take into account grain failure. Compared to the
475 framework introduced by Thornton and Ning (1998) [43], the granule elastic limit in the present
476 study is given in term of a "limiting contact force", given by R_A , directly obtained from
477 experimental results [36], instead of a "limiting contact pressure". Pellet failure in the simulation
478 is thus taken into account by introducing perfect plasticity in the contact law, with the pellet

479 strength decreasing upon hydration (equation (4)). The mean value of the ratio of total
480 deflection to particle diameter using this approach is lower than 0.07.

481

482 However, it is worth mentioning that experimental results evidenced a decrease of normal force
483 at failure (constant suction) [36], which is not taken into account by the perfect plasticity of the
484 contact behaviour adopted in the present study. Nevertheless, the calculated swelling pressure
485 for suctions at which most of the contacts had reached the elastic limit appeared to be in the
486 right order of magnitude.

487

488 Modelling the swelling of spherical particles within a granular assembly by a radius increase has
489 already been performed in DEM, for super absorbent polymer hydration [35] or thermal
490 expansion effect in granular materials [33, 34]. In these works, a water/heat transfer was
491 introduced and the particles would swell accordingly. In the present work, the approach is
492 slightly different because no transfer law is introduced. All particles swell simultaneously,
493 suction is calculated from equation (3) and all mechanical parameters vary accordingly. It is
494 based on the assumption that vapour diffusion in inter-pellet porosity occurs significantly faster
495 than absorption of water by pellets. The macropores are thought to be full of air at the same
496 relative humidity. From Figure 10a and 10b, it can be observed that the macroporosity is still
497 clearly observable at 4 MPa of suction. In addition, humid air is free to enter the sample
498 macroporosity from either the bottom or the top of the cell (Figure 3). It is thus thought that the
499 suction value imposed to all granules is identical within the isochoric cell. In addition, it is also
500 suggested that there is still free volume available for the pellets to swell.

501

502 The model is able to reproduce the general “two phases” trend of the swelling pressure
503 development observed in the laboratory (DEM1 in Figure 9). The first phase, characterised by a
504 sharp increase of swelling pressure until a peak value is reached, is however overestimated by
505 the model. The overestimation of the swelling pressure at high suction in simulation is a
506 consequence of several features: the modelled beads are all identically shaped (perfect spheres
507 of same diameter), cannot rearrange as a consequence of the small cell size ($H_{\text{cell}} / a_{\text{eq}} = 4$),
508 and have the same mechanical properties.

509

510 It is highlighted in [36] that the variability of pellet mechanical properties is more important at
511 high suction. According to equation (8), the contact force is proportional to the pellet stiffness if
512 all pellets have the same stiffness. In case of a stiffness variability between two pellets in
513 contact, the term $E_m / 1 - \nu^2$ in equations (8) would be given by [37]:

514

$$(17) \quad \frac{E_m}{1 - \nu^2} = \frac{1}{\frac{1 - \nu_1^2}{E_{m1}} + \frac{1 - \nu_2^2}{E_{m2}}}$$

515

516 Where E_{m1} , E_{m2} , ν_1 and ν_2 are the Young modulus of pellet 1 and pellet 2 and the Poisson ratio
517 of pellet 1 and 2 in the contact. Equation (17) highlights that the contact stiffness would be
518 significantly smaller if the Young modulus of one of the pellets in contact were smaller.

519

520 The second phase, at lower suction, and lower variability of the mechanical properties, is closer
521 to experimental results. During the second phase, the initial features of the granular assembly
522 have less influence on the macroscopic response because contact forces have reached the
523 elastic limit and the swelling pressure mainly depends on the pellet strength and stiffness
524 decreases upon suction decrease. Thus, swelling pressures in DEM1, DEM2, and DEM3 have
525 comparable values. “Two phases” trends had already been obtained for Febex granular
526 bentonite [19, 30]. In these studies the swelling pressure would increase then remain nearly
527 constant until final saturation (zero suction). It was also suggested that the “plateau” swelling
528 pressure value was a consequence of the pellet strength and stiffness decrease upon hydration.

529

530 In the present study, pellet initial diameter is 7 mm. To model pellets of a different size, the
531 simulation method can directly be applied as long as the aforementioned conditions for model
532 validity are verified. Pellet mechanical properties are likely to be influenced by the pellet size
533 [36]. These latter should thus be carefully determined before modelling pellets of different size.

534

535 **5.2. Limit of the proposed framework at low suction**

536

537 Wang et al. (2012) [8] proposed an estimation of the final swelling pressure of a compacted
538 bentonite-based material from its initial dry density. From this estimation, the final swelling
539 pressure of the studied material is ~0.21 MPa, higher than the “plateau” value obtained in the
540 swelling pressure tests. The swelling pressure is thus expected to increase upon further suction
541 decrease. Compacted bentonite materials display a change in the hydration and swelling
542 mechanism at low suction. Saiyouri et al. (2004) [47] evidenced that the water uptake
543 mechanisms of compacted MX80 bentonite materials undergo a significant change between ~3
544 and ~7 MPa of suction. This suction range coincides with a sharp irreversible decrease of the
545 number of layers by clay particle. The proportion of interparticle porosity increases, diffuse
546 double layers are thought to develop and the proportion of interparticle water considerably
547 increases. This is consistent with the transition from the microstructural domain to a dry density-
548 dependent domain of the water retention curve of MX80-based materials [4] and the pore
549 volume reorganisation of MX80 pellets [48].

550

551 The DEM model would be unable to reproduce this behaviour and is considered not to be
552 appropriate to describe the swelling pressure evolution upon suction decrease below this
553 threshold (between ~3 and ~7 MPa of suction), even if the material remains granular below
554 these values (Figure 10a and 10b).

555

556 **5.3. Influence of walls on the measured response**

557

558 Vargas and McCarthy (2007) [30] performed simulations of particles swelling in both a fixed-
559 walls and a free moving-walls cell. In the first case, particle swelling induced an increase of
560 contact force instead of particle rearrangement. In the second case, the mean contact force was
561 not significantly increasing upon particle radius increase. These two extreme cases highlight
562 that the more particles rearrange, the more the coordination number will increase and the less
563 contact forces will.

564

565 The evolution of the mean elastic normal deflection upon radius increase, at contact between
566 pellets and the upper wall, is presented in Figure 16. DEM1 results (optimised preparation and

567 friction during hydration) are characterised by a nearly perfect linear deflection-radius variations
568 relationship until reaching the peak swelling pressure. The linear relationship between these two
569 parameters is close to the " $\Delta\delta_N^e = \Delta R$ " line which implies negligible rearrangement of the
570 granular assembly upon swelling. The swelling pressure increase is thus significant and elastic
571 limit in contacts with the upper wall is reached almost simultaneously, resulting in an
572 overestimated peak value and an accentuated transition between phases 1 and 2. This
573 tendency towards deflection increase instead of particle rearrangement in the simulations is
574 also underlined in Figure 16 by the significant increase of the mean elastic normal deflection
575 after the cell closure in DEM2 (friction during preparation). The considered solid fraction (0.553)
576 is low and these features should not be observed in larger granular assemblies, less influenced
577 by walls. Since pellet-wall contacts are stiffer than pellet-pellet contacts, negligible
578 rearrangements also explain the more significant increase in contact plasticity at contact with
579 walls compared to the mean increase in the samples. As a consequence, the post-peak
580 decrease of swelling pressure can be overestimated if swelling pressure is measured at contact
581 with the wall instead of calculating the mean stress in the sample (Figure 17).

582
583 The influence of the walls is furthermore underlined by the coordination number following
584 preparation (Figure 12): the coordination number of frictionless bead assemblies was 5.4
585 instead of the bulk value ~ 6 [41].

586
587 These results suggest that the variability associated to sample preparation stems from wall
588 influence. Experimental tests are influenced by the walls as well, because they share the same
589 solid fraction and $H_{cell} / a_{eq 0}$ ratio.

590

591 **5.4. Contribution of DEM to laboratory testing**

592

593 Thanks to the DEM ability to model the wall-pellet interaction and access grain-scale
594 phenomena, simulation results can provide an insight into swelling pressure tests carried out at
595 laboratory scale, especially since walls have non-negligible influence on the measured
596 response.

597

598 The influence of sample preparation on test results was highlighted by DEM simulations (Figure
599 9). The general trend of DEM2 results suggests that initial pressure required to close the cell
600 before hydration can cause a significant increase of plastic contact proportion (Figure 11b). As a
601 consequence, hydration phase 1 appeared very limited in DEM2. The sample behaviour was
602 mainly controlled by equations (2) and (4) and the number of contacts between pellets and the
603 upper wall, rather than the particle swelling. Even if plasticity does not arise during the closure
604 step, closure can have an influence on the behaviour upon hydration. At granular state, the
605 mean stress in the sample is proportional to the product of coordination number and mean
606 contact force. It was highlighted in Figure 12 that the evolution of the coordination number was
607 not influenced by the sample preparation. Thus, samples prepared under higher initial closure
608 pressure are likely to reach plasticity more rapidly. This is actually suggested by SP1 and SP2
609 test results. It is recommended that the control of the initial state is as important as the value of
610 the sample density to study the swelling pressure development of pellet materials.

611

612 Beside variability arising from wall influence, small pressure sensors in the laboratory have
613 been shown to induce additional variability of the measured swelling pressure. DEM allowed the
614 influence of the pressure sensor diameter on the variability of the measured swelling pressure
615 to be quantified. This variability, along with the variability of behaviour associated to the sample
616 small size, increases the difficulty to study the intrinsic behaviour of pellet mixtures at laboratory
617 scale. For granules with the same mechanical behaviour, the coefficient of variation of swelling
618 pressure obtained from simulations thus depends on both the preparation in a small cell and the
619 ratio of sensor diameter to pellet diameter.

620

621 It was discussed that an overestimation of the calculated swelling pressure can arise in the
622 elastic phase of the granule swelling from some of the model simplifications, especially at the
623 highest suction values. However, concerning the variability of this measure, these
624 simplifications can reduce the coefficient of variation. Owing to the dispersion of the granule real
625 mechanical properties at high suctions, the calculated coefficient of variation associated to
626 swelling pressure is likely to be underestimated by the model in the elastic part of the hydration

627 path. As contact forces reach the elastic limit, normal forces reach less dispersed values and
628 the calculated coefficient of variation decreases.

629

630 These results are of importance, since most of the time the material behaviour is studied at
631 laboratory scale, with inevitable constraints concerning the number and sizes of sensors,
632 related to the cell size. It is recommended that experiments performed to determine material
633 parameters for modelling purpose should be interpreted carefully considering the order of
634 magnitude of the variability.

635

636 Simulation results highlighted the influence of interactions at contacts between pellets on the
637 material behaviour upon hydration. Since pellets would lose their structure upon full saturation,
638 the material behaviour is sensitive to the hydration method at laboratory scale. The influence of
639 the granular nature of the material is likely to be underestimated upon fast liquid water
640 hydration.

641

642 **5.5. Contribution of DEM to constitutive modelling of pellet materials**

643

644 The proposed DEM model has been shown to reproduce the main features of the material
645 behaviour upon partial hydration in constant-volume conditions. The relationships between the
646 behaviour of the granules and the macrostructural behaviour can be identified. It can provide
647 valuable information for the modelling of pellet mixture behaviour using double structure
648 models. This modelling framework has been used in previous studies to model pellet materials
649 upon hydration, considering the pellet phase as the microstructure [20, 21, 23].

650

651 For this purpose, DEM can be a complementary tool to experimental studies. It was highlighted
652 that results of experimental tests performed at the laboratory scale on pellet mixtures can be
653 characterised by a significant variability. This latter can make the determination of the material
654 intrinsic behaviour difficult. DEM allows uncertainty and variability to be taken into account, at
655 low simulation cost. DEM model parameters can be determined from experimental tests at the

656 pellet scale [36]. Then, the model can be validated against swelling pressure tests or other
657 common tests at the laboratory scale.

658

659 Simulations may be performed in conditions where the intrinsic behaviour of the material can be
660 addressed. DEM could help determining constitutive laws for the mechanical behaviour of a
661 pellet assembly and relationship between pellet swelling and pellet assembly swelling. In this
662 respect, a perspective arising from the present study results is to perform DEM simulations of
663 large pellet assemblies of different solid fractions upon hydration, avoiding the influence of wall
664 and small sample sizes. In this way, constitutive laws describing the material before
665 homogenisation could be proposed and integrated in a double structure model.

666

667

668 **6. Conclusions**

669

670 The hydromechanical behaviour of pellet assemblies was studied through laboratory and DEM-
671 simulated swelling pressure tests. DEM model parameters were obtained from pellet scale
672 experimental characterisation. The DEM model was validated against experimental results.
673 Numerical results allowed the experimental results to be interpreted with respect to grain scale
674 phenomena.

675

676 Compared to traditional compacted powder materials, pellet materials are characterised by an
677 initial granular nature, which was shown in the present study to control the material behaviour
678 upon hydration to suction as low as 4 MPa. In particular, it was shown that, in constant volume
679 conditions, the granule strength and stiffness control the macroscopic response. Upon
680 hydration, the swelling pressure develops in two phases. The first is characterised by an elastic
681 increase of the normal contact forces and is affected by the initial state of the material, thus the
682 sample preparation in laboratory tests. The second is characterised by the occurrence of
683 contact plasticity and is less affected by the initial state.

684

685 DEM simulations satisfactorily reproduced the material behaviour observed at laboratory scale.
686 DEM results suggest that the 30 mm x 60 mm isochoric cell ($H_{cell} / a_{eq,0} = 4$) was not a true
687 representative elementary volume, due to its small size and the significant influence of the
688 walls. In addition, it was shown that a low value of the ratio of sensor diameter to pellet diameter
689 induces significant measurement variability in the investigated suction range.

690

691 A perspective arising from the present study is the DEM modelling of large pellet assemblies
692 upon hydration, with no influence of the walls. Constitutive laws for the material before
693 homogenisation could be proposed and provide an interesting framework for further FEM
694 simulations of the entire hydration path, using double structure models in which pellets could be
695 considered as the microstructural phase.

696

697

698 **Conflict of Interest:**

699

700 The authors declare that they have no conflict of interest.

701

702

703 **References**

704

705 1. Blatz JA, Graham J, Chandler NA (2002) Influence of suction on the strength
706 and stiffness of compacted sand–bentonite. Can Geotech J 39:1005–1015.

707 <https://doi.org/10.1139/t02-056>

708 2. Lloret A, Villar M V, Sanchez M, et al (2003) Mechanical behaviour of heavily
709 compacted bentonite under high suction changes. Geotechnique 53:27–40.

710 <https://doi.org/10.1680/geot.53.1.27.37258>

711 3. Agus SS, Schanz T (2005) Effect of Shrinking and Swelling on Microstructures
712 and Fabric of a Compacted Bentonite-Sand Mixture. Proc Int Conf Probl Soils, 25-27 May 2005,

713 East Mediterr Univ Famagusta, N Cyprus

- 714 4. Villar M V. (2007) Water retention of two natural compacted bentonites. *Clays*
715 *Clay Miner* 55:311–322. <https://doi.org/10.1346/CCMN.2007.0550307>
- 716 5. Saiyouri N, Hicher PY, Tessier D (2000) Microstructural approach and transfer
717 water modelling in highly compacted unsaturated swelling clays. *Mech Cohesive-frictional Mater*
718 5:41–60
- 719 6. Delage P, Marcial D, Ruiz X, Cui YJ (2006) Ageing effects in a compacted
720 bentonite: a microstructure approach. *Géotechnique* 56:291–304.
721 <https://doi.org/10.1680/geot.2006.56.5.291>
- 722 7. Tang, AM, Cui YJ, Le TT (2008) A study on the thermal conductivity of
723 compacted bentonites. *Appl Clay Sci* 41:181–189
- 724 8. Wang Q, Tang AM, Cui YJ, et al (2012) Experimental study on the swelling
725 behaviour of bentonite/claystone mixture. *Eng Geol* 124:59–66.
726 <https://doi.org/10.1016/j.enggeo.2011.10.003>
- 727 9. Saba S, Cui Y, Tang AM, Barnichon J (2014) Investigation of the swelling
728 behaviour of compacted bentonite-sand mixtures by mock-up tests. *Can Geotech J* 51:1399–
729 1412
- 730 10. Sun H, Mašín D, Najser J, et al (2019) Bentonite microstructure and saturation
731 evolution in wetting-drying cycles evaluated using ESEM, MIP and WRC measurements.
732 *Geotechnique* 69:713–726. <https://doi.org/10.1680/jgeot.17.P.253>
- 733 11. Seiphoori A, Ferrari A, Laloui L (2014) Water retention behaviour and
734 microstructural evolution of MX-80 bentonite during wetting and drying cycles. *Géotechnique*
735 64:721–734. <https://doi.org/10.1680/geot.14.P.017>
- 736 12. Massat L, Cuisinier O, Bihannic I, et al (2016) Swelling pressure development
737 and inter-aggregate porosity evolution upon hydration of a compacted swelling clay. *Appl Clay*
738 *Sci* 124–125:197–210. <https://doi.org/10.1016/j.clay.2016.01.002>
- 739 13. Keller LM, Seiphoori A, Gasser P, et al (2014) The pore structure of compacted
740 and partly saturated MX-80 bentonite at different dry densities. *Clays Clay Miner* 62:174–187.
741 <https://doi.org/10.1346/CCMN.2014.0620302>
- 742 14. Komine H, Ogata N (2003) New equations for swelling characteristics of
743 bentonite-based buffer materials. *Can Geotech J* 40:460–475. <https://doi.org/10.1139/t02-115>

- 744 15. Cuisinier O, Masroui F (2005) Hydromechanical behaviour of a compacted
745 swelling soil over a wide suction range. *Eng Geol* 81:204–212.
746 <https://doi.org/10.1016/j.enggeo.2005.06.008>
- 747 16. Karnland O, Nilsson U, Weber H, Wersin P (2008) Sealing ability of Wyoming
748 bentonite pellets foreseen as buffer material - Laboratory results. *Phys Chem Earth* 33:472–
749 475. <https://doi.org/10.1016/j.pce.2008.10.024>
- 750 17. Volckaert, G., Bernier, F., Alonso, E. E., et al (1996). Thermal-hydraulic-
751 mechanical and geochemical behaviour of the clay barrier in radioactive waste repositories
752 (model development and validation), EUR 16744 EN. Luxembourg: Publications of the
753 European Communities.
- 754 18. van Geet M, Volckaert G, Roels S (2005) The use of microfocus X-ray
755 computed tomography in characterising the hydration of a clay pellet/powder mixture. *Appl Clay*
756 *Sci* 29:73–87. <https://doi.org/10.1016/j.clay.2004.12.007>
- 757 19. Hoffmann C, Alonso EE, Romero E (2007) Hydro-mechanical behaviour of
758 bentonite pellet mixtures. *Phys Chem Earth* 32:832–849.
759 <https://doi.org/10.1016/j.pce.2006.04.037>
- 760 20. Alonso EE, Romero E, Hoffmann C (2011) Hydromechanical behaviour of
761 compacted granular expansive mixtures: experimental and constitutive study. *Géotechnique*
762 61:329–344. <https://doi.org/10.1680/geot.2011.61.4.329>
- 763 21. Gens A, Valleján B, Sánchez M, et al (2011) Hydromechanical behaviour of a
764 heterogeneous compacted soil: experimental observations and modelling. *Géotechnique*
765 61:367–386. <https://doi.org/10.1680/geot.SIP11.P.015>
- 766 22. Molinero-Guerra A, Mokni N, Delage P, et al (2017) In-depth characterisation of
767 a mixture composed of powder/pellets MX80 bentonite. *Appl Clay Sci* 135:538–546.
768 <https://doi.org/10.1016/j.clay.2016.10.030>
- 769 23. Mokni N, Molinero-Guerra A, Cui Y-J, et al (2019) Modelling the long-term
770 hydro-mechanical behaviour of a bentonite pellet/powder mixture with consideration of initial
771 structural heterogeneities. *Géotechnique* 1–61. <https://doi.org/10.1680/jgeot.18.p.110>

- 772 24. Zhang Z, Ye W, Liu Z, et al (2020) Mechanical behavior of GMZ bentonite pellet
773 mixtures over a wide suction range. *Eng Geol* 264:105383.
774 <https://doi.org/10.1016/j.enggeo.2019.105383>
- 775 25. Liu Z, Ye W, Zhang Z, et al (2019) Particle size ratio and distribution effects on
776 packing behaviour of crushed GMZ bentonite pellets. *Powder Technol* 351:92–101.
777 <https://doi.org/10.1016/j.powtec.2019.03.038>
- 778 26. Liu, Z., Cui, Y., Ye, W. et al (2020) Investigation of the hydro-mechanical
779 behaviour of GMZ bentonite pellet mixtures. *Acta Geotech*. [https://doi.org/10.1007/s11440-020-](https://doi.org/10.1007/s11440-020-00976-y)
780 [00976-y](https://doi.org/10.1007/s11440-020-00976-y)
- 781 27. Molinero-Guerra A, Aïmedieu P, Bornert M, et al (2018) Analysis of the
782 structural changes of a pellet/powder bentonite mixture upon wetting by X-ray computed
783 microtomography. *Appl Clay Sci* 165:164–169. <https://doi.org/10.1016/j.clay.2018.07.043>
- 784 28. Yigzaw ZG, Cuisinier O, Massat L, Masroui F (2016) Role of different suction
785 components on swelling behavior of compacted bentonites. *Appl Clay Sci* 120:81–90.
786 <https://doi.org/10.1016/j.clay.2015.11.022>
- 787 29. Imbert C, Villar MV (2006) Hydro-mechanical response of a bentonite
788 pellets/powder mixture upon infiltration. *Appl Clay Sci* 32:197–209.
789 <https://doi.org/10.1016/j.clay.2006.01.005>
- 790 30. Molinero Guerra A, Cui YJ, Mokni N, et al (2018) Investigation of the hydro-
791 mechanical behaviour of a pellet/powder MX80 bentonite mixture using an infiltration column.
792 *Eng Geol* 243:18–25. <https://doi.org/10.1016/j.enggeo.2018.06.006>
- 793 31. Alonso EE, Hoffmann C, Romero E (2010) Pellet mixtures in isolation barriers.
794 *J Rock Mech Geotech Eng* 2:12–31. <https://doi.org/10.3724/SP.J.1235.2010.00012>
- 795 32. Radjai, F. & Dubois, F. (2011). *Discrete-element modeling of granular*
796 *materials*. Wiley-ISTE, ISBN 978-1-84821-260-2.
- 797 33. Vargas WL, McCarthy JJ (2007) Thermal expansion effects and heat
798 conduction in granular materials. *Phys Rev E - Stat Nonlinear, Soft Matter Phys* 76:1–8.
799 <https://doi.org/10.1103/PhysRevE.76.041301>

- 800 34. Zhao S, Evans TM, Zhou X, Zhou S (2017) Discrete element method
801 investigation on thermally-induced shakedown of granular materials. *Granul Matter* 19:1–11.
802 <https://doi.org/10.1007/s10035-016-0690-5>
- 803 35. Sweijen T, Chareyre B, Hassanizadeh SM, Karadimitriou NK (2017) Grain-
804 scale modelling of swelling granular materials; application to super absorbent polymers. *Powder*
805 *Technol* 318:411–422. <https://doi.org/10.1016/j.powtec.2017.06.015>
- 806 36. Darde B, Tang AM, Pereira J-M, et al (2018) Hydro-mechanical behaviour of
807 high-density bentonite pellet on partial hydration. *Géotechnique Lett* 8:330–335.
808 <https://doi.org/10.1680/jgele.18.00114>
- 809 37. Johnson KL (1985) *Contact Mechanics*. Cambridge University Press,
810 Cambridge, UK
- 811 38. Darde B, Tang AM, Roux JN, et al (2020) Effects of the initial granular structure
812 of clay sealing materials on their swelling properties : experiments and DEM simulations. *EPJ*
813 *Nuclear Sci. Technol.* 6. <https://doi.org/10.1051/epjn/2019059>.
- 814 39. Tang A-M, Cui Y-J (2005) Controlling suction by the vapour equilibrium
815 technique at different temperatures and its application in determining the water retention
816 properties of MX80 clay. *Can Geotech J* 42:287–296. <https://doi.org/10.1139/t04-082>
- 817 40. Agnolin I, Roux JN (2007) Internal states of model isotropic granular packings.
818 I. Assembling process, geometry, and contact networks. *Phys Rev E - Stat Nonlinear, Soft*
819 *Matter Phys* 76:1–27. <https://doi.org/10.1103/PhysRevE.76.061302>
- 820 41. Roux J-N (2000) Geometric origin of mechanical properties of granular
821 materials. *Phys Rev E - Stat Nonlinear, Soft Matter Phys* 61:1–35
- 822 42. Wiacek J, Molenda M, Horabik J, Ooi JY (2012) Influence of grain shape and
823 intergranular friction on material behavior in uniaxial compression: Experimental and DEM
824 modeling. *Powder Technol* 217:435–442. <https://doi.org/10.1016/j.powtec.2011.10.060>
- 825 43. Thornton C, Ning Z (1998) A theoretical model for the stick/bounce behaviour of
826 adhesive, elastic- plastic spheres. *Powder Technol* 99:154–162. [https://doi.org/10.1016/S0032-](https://doi.org/10.1016/S0032-5910(98)00099-0)
827 [5910\(98\)00099-0](https://doi.org/10.1016/S0032-5910(98)00099-0)

828 44. Thornton C, Cummins SJ, Cleary PW (2017) On elastic-plastic normal contact
829 force models, with and without adhesion. *Powder Technol* 315:339–346.
830 <https://doi.org/10.1016/j.powtec.2017.04.008>

831 45. Bolton MD, Nakata Y, Cheng YP (2008) Micro- and macro-mechanical
832 behaviour of DEM crushable materials. *Géotechnique* 58:471–480.
833 <https://doi.org/10.1680/geot.2008.58.6.471>

834 46. Cheng YP, Bolton MD, Nakata Y (2004) Crushing and plastic deformation of
835 soils simulated using DEM. *Géotechnique* 54:131–141.
836 <https://doi.org/10.1680/geot.2004.54.2.131>

837 47. Saiyouri N, Tessier D, Hicher PY (2004) Experimental study of swelling in
838 unsaturated compacted clays. *Clay Miner* 39:469–479.
839 <https://doi.org/10.1180/0009855043940148>

840 48. Molinero-Guerra A, Delage P, Cui Y-J, et al (2019) Water retention properties
841 and microstructure changes of a bentonite pellet upon wetting/drying; application to radioactive
842 waste disposal. *Géotechnique* 1–41. <https://doi.org/10.1680/jgeot.17.p.291>
843
844

845 **List of symbols**

846

847 a_{eq0} : initial sphere diameter in the simulations

848 a_{eqi} : sphere diameter at step i in the simulations

849 a_{eq} : sphere diameter in the simulations

850 C_A : model parameter

851 D_0 : initial diameter of the pellet

852 D_{sensor} : diameter of the pressure sensor

853 E_m : pellet Young modulus

854 F_{max} : maximum normal force on a particle

855 F_N : normal contact elastic force

856 F_{net} : net force on a particle

857 F_T : norm of the tangential reaction vector

858 \mathbf{F}_T : tangential reaction vector

859 $\dot{\mathbf{F}}_T$: increment of tangential reaction vector

860 h_0 : initial height of the cylinder-shaped part of the pellet

861 H_0 : initial total height of the pellet

862 H_{cell0} : initial height of the cylinder

863 H_{cell} : height of the cylinder during the swelling step

864 m : mean value

865 m_p : mass of the pellet

866 N_{c1} : number of particle-particle contacts

867 N_{c2} : number of particle-wall contacts

868 N_p : number of particles

869 N^v : viscous component of the contact force

870 p^* : effective mean stress

871 P_S^* : apparent swelling pressure at equilibrium in the simulations

872 P_{SXP} : axial pressure in swelling pressure tests

873 R_A : pellet strength

874 R_c : curvature radius of the pellet

875 s_0 : initial suction of the pellet

876 V : volume of the pellet

877 w_0 : initial water content of the pellet

878 $x_{c\ sup}^p$: evolution of the mean plastic contacts proportion for contacts between pellets and the
879 upper wall

880 $x_{c\ tot}^p$: evolution of the mean plastic contacts proportion for the whole sample

881 Z: coordination number

882 α_m : model parameter

883 α_v : Damping parameter

884 β_m : model parameter

885 Γ_{max} : maximum moment on a particle

886 Γ_{net} : net moment on a particle

887 δ_N^e : normal elastic deflection at contact

888 $\Delta\delta_N^e$: variation of the mean normal elastic deflection during particle swelling

889 ΔR : variation of the particle radius during swelling

890 δ_T : relative tangential displacement vector

891 δ_T : increment of relative tangential displacement vector

892 ϵ : tolerance value for equilibrium in the simulations

893 λ_i : parameter describing the diameter increment at step i in DEM

894 λ_0 : parameter describing the diameter increment at initial state in DEM

895 λ_f : parameter describing the diameter increment at final state in DEM

896 ϵ_{vm} : pellet volumetric strain

897 μ : friction coefficient

898 ν : pellet Poisson ratio

899 ρ_{d0} : initial dry density of the pellet

900 ρ_s : MX80 particle density

901 σ : standard deviation

902

903

904

905 **TABLES AND TABLE CAPTIONS**

906

907 **TABLE 1** Properties of the MX80 bentonite

908

Property	Value
Particle density, ρ_s (g/cm ³)	2.77
Smectite content (%)	80
Liquid limit (%)	560
Plastic limit	53
CEC (meq/g)	98/100

909

910

911 **TABLE 2** Initial properties of the granules

912

Property	Value
Dry density, ρ_{d0} (Mg/m ³)	1.90
Water content, w_0 (%)	12.2
Diameter, D_0 (mm)	7.0
Height, H_0 (mm)	7.0
Height of the cylinder-shaped part, h_0 (mm)	5.0
Curvature radius, R_c (mm)	6.5
Suction, s_0 (MPa)	89

913

914

915

916 **TABLE 3** Geometrical properties of isochoric cells

917

Property	Value
Sample height, H_{cell} (mm)	30
Sample diameter, D_{cell} (mm)	60
Sensor diameter, D_{sensor} (mm)	30
Sample volume (mm ³)	84823

918

919

920 **TABLE 4** Suction values imposed using the vapour equilibrium technique

921

Salt solution	Suction (MPa)
Mg(NO ₃) ₂	82
NH ₄ NO ₃	59
NaNO ₃	40
NaCl	38
(NH ₄) ₂ SO ₄	25
Na ₂ CO ₃	13
KNO ₃	9
K ₂ SO ₄	4

922

923

924 **TABLE 5** Friction values used during preparation and hydration steps in DEM1, DEM2 and
 925 DEM3 simulations. 100 simulations are performed for each type of simulation

926

Simulation	μ (preparation step) (-)	μ (swelling step) (-)
DEM01	0	0.3
DEM02	0.3	0.3
DEM03	0	0

927

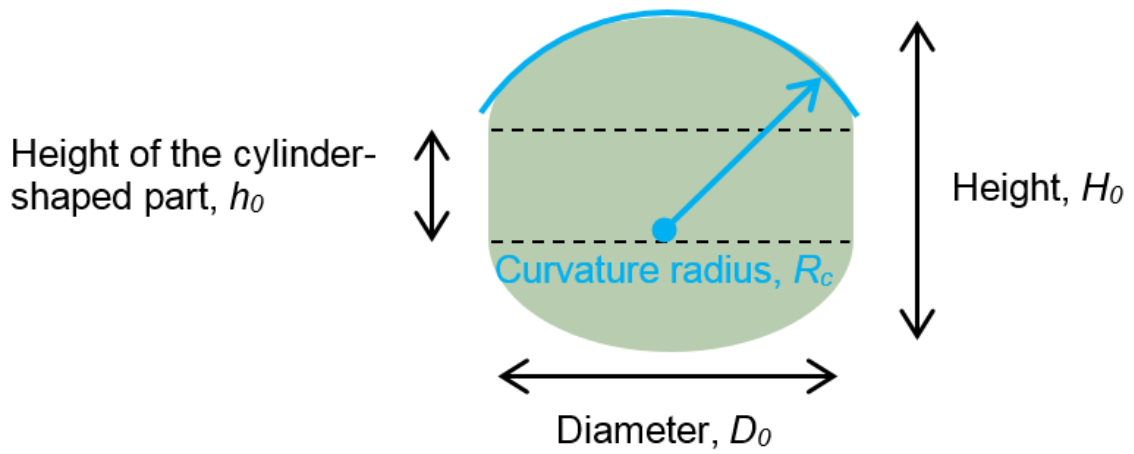
928

929 FIGURES AND FIGURE CAPTIONS

930

931 Fig. 1 Schematic view of a pellet

932



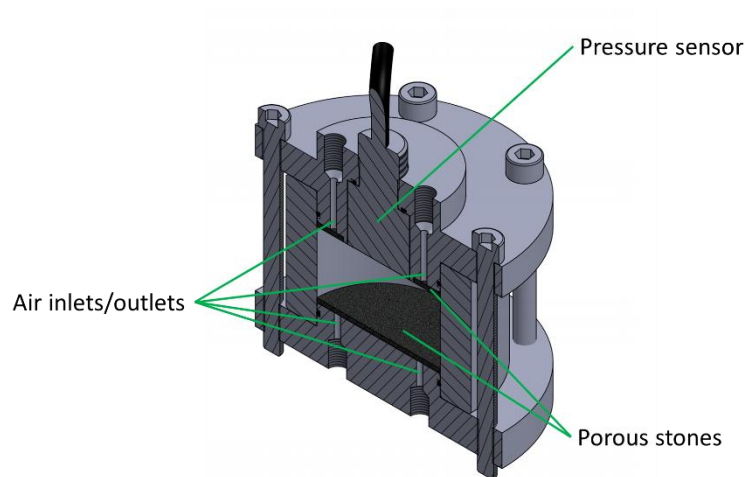
933

934

935

936 Fig. 2 Isochoric cell used for swelling pressure tests

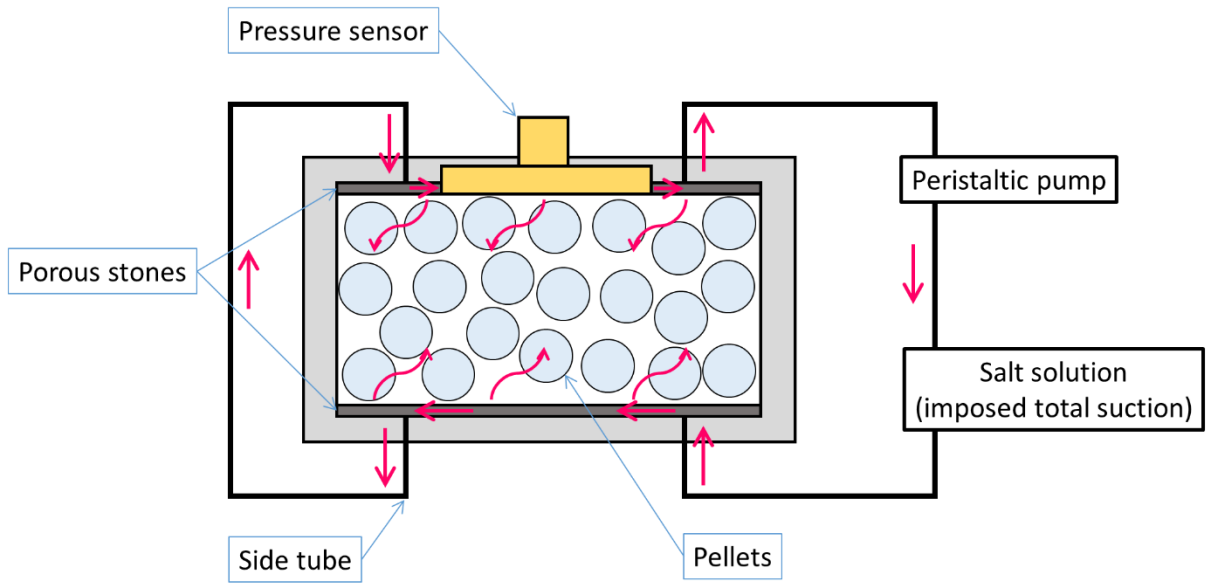
937



938

939

940 **Fig. 3** Air circulation in the isochoric cell
941

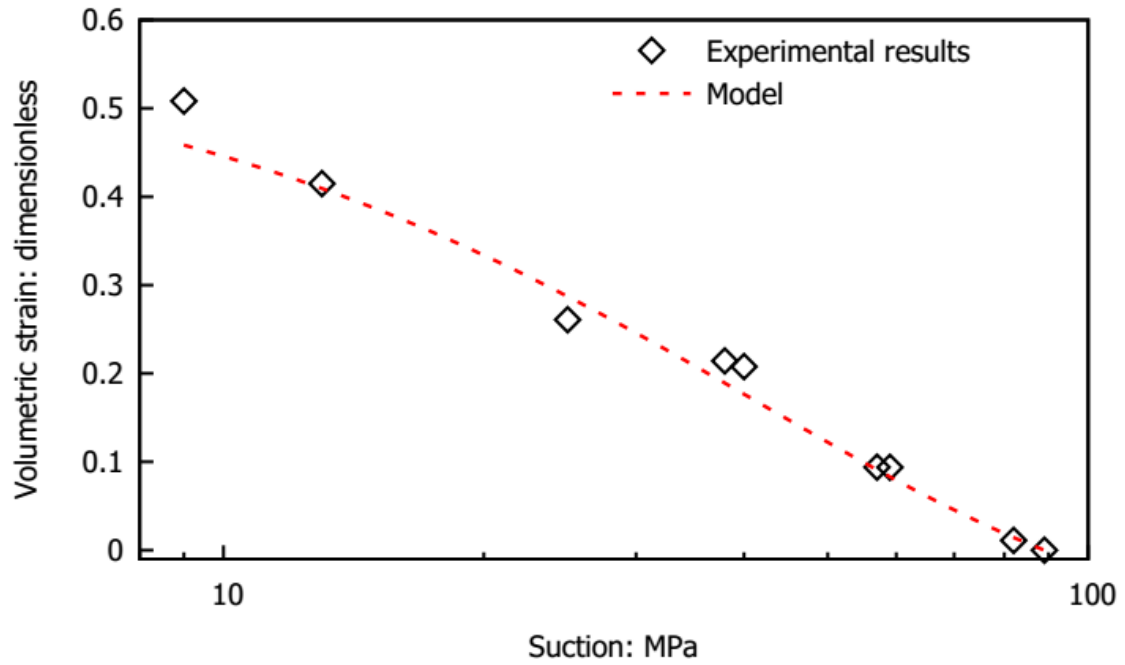


942
943
944

945

946 **Fig. 4a** Hydromechanical behaviour of a pellet (Darde et al., 2018). a) Evolution of Volumetric strain upon suction decrease for one pellet
947

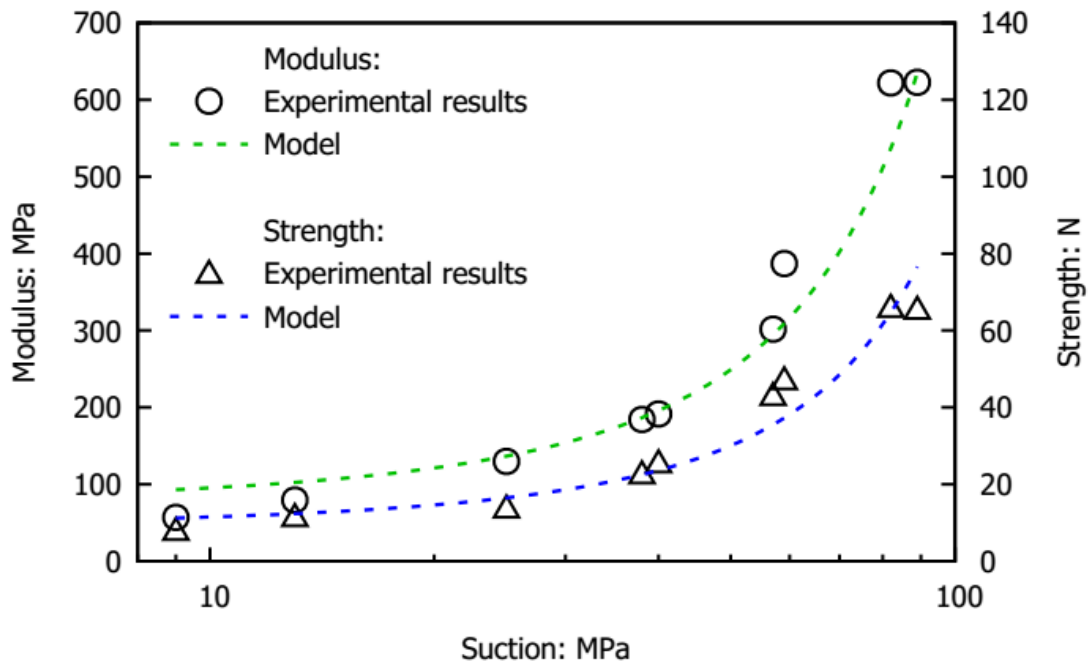
948



949

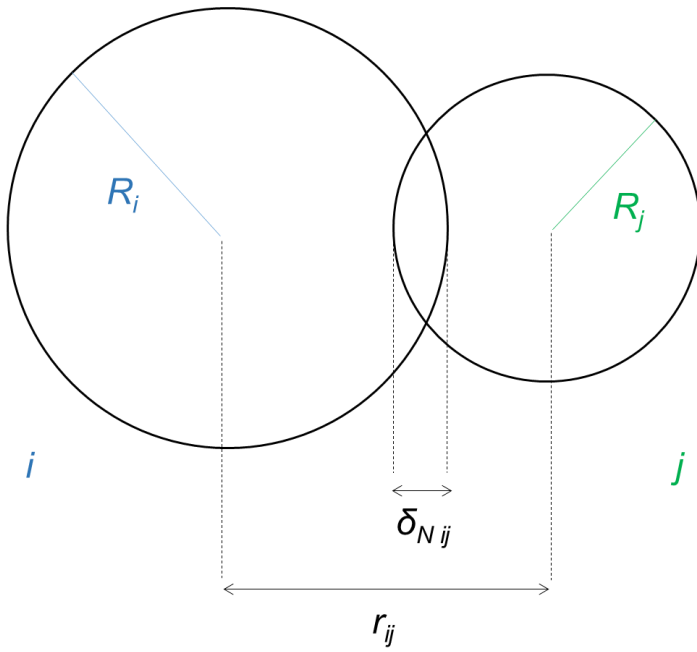
950

951 **Fig. 4b** Evolution of Modulus and Strength upon suction decrease for one pellet
952



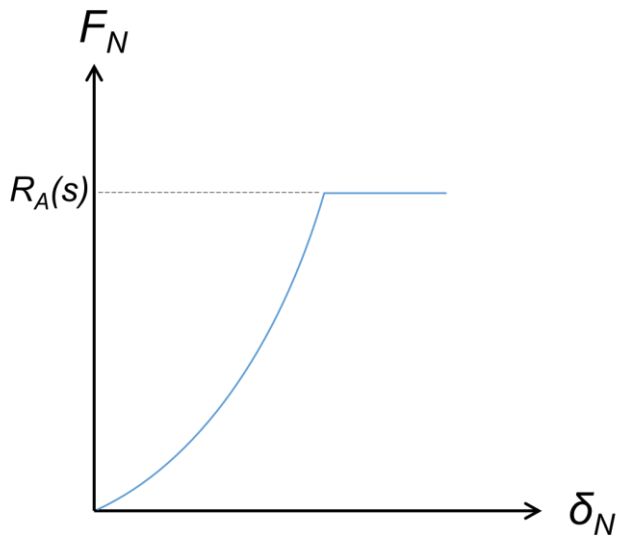
953
954
955
956

957 **Fig. 5** Contact between two particles in DEM
958



959
960
961
962

963 **Fig. 6a** Contact laws used in the model: Normal reaction: Hertz law + perfect plasticity
964

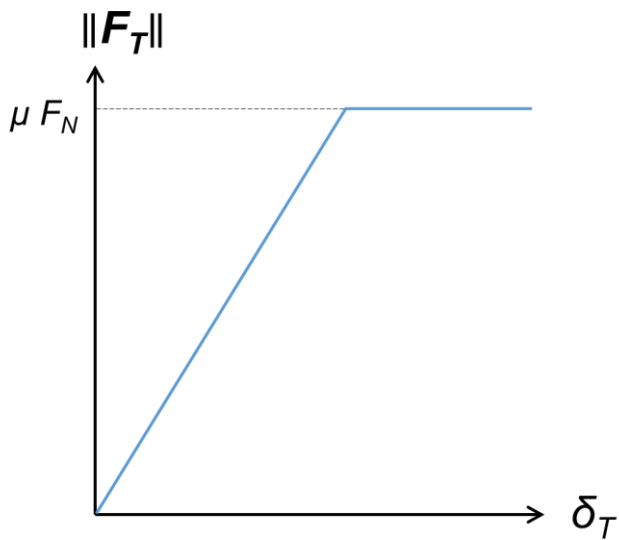


965

966

967 **Fig 6b** Tangential reaction: Simplified elasticity law + Coulomb friction

968



969

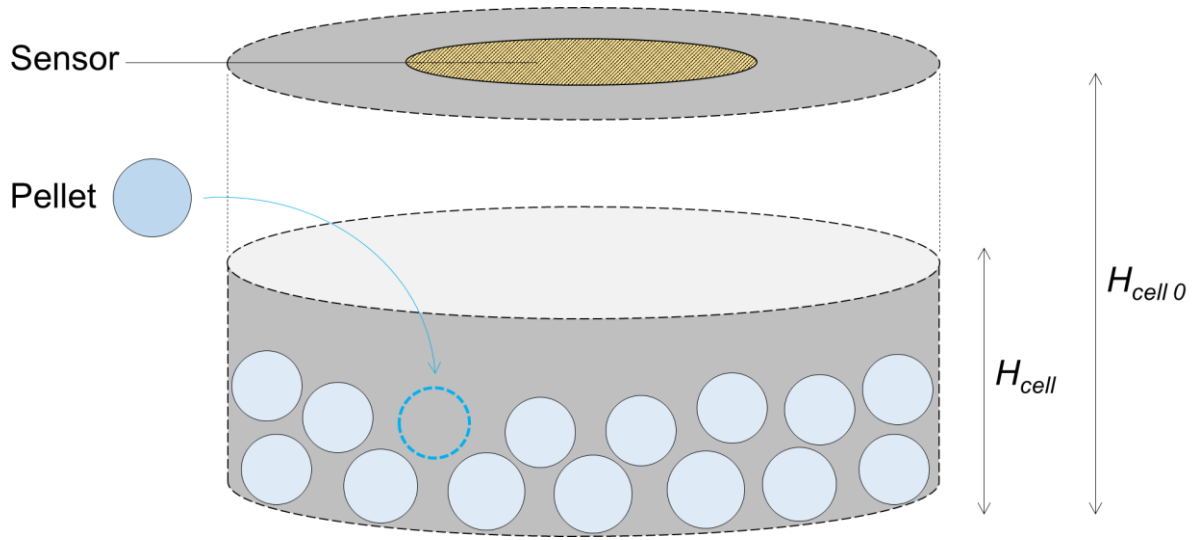
970

971

972

973 **Fig. 7a** Preparation step in DEM

974



975

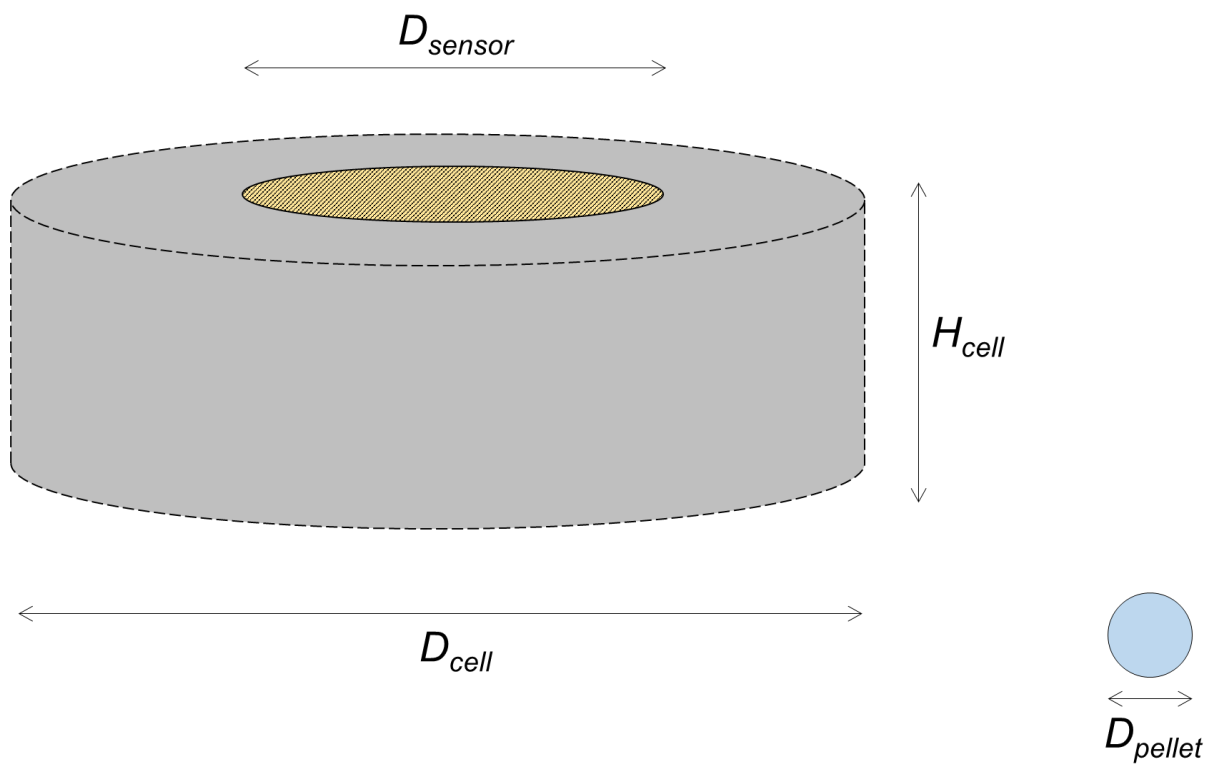
976

977

978

979 **Fig. 7b** Dimensions of the isochoric cell

980



981

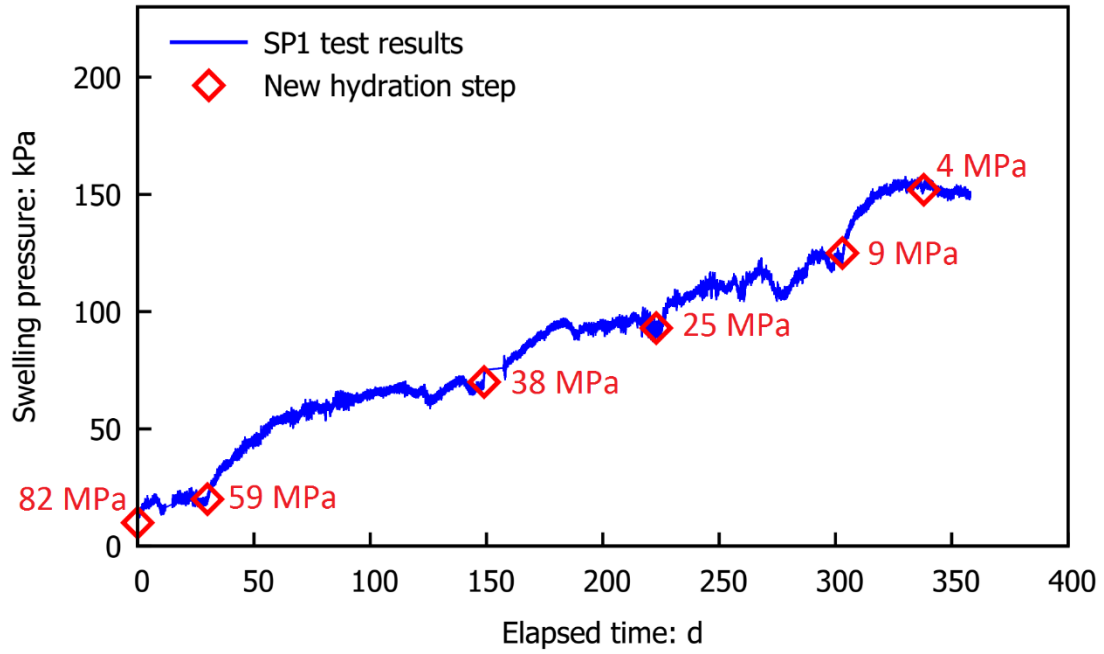
982

983

984

985 **Fig. 8a** Swelling pressure as a function of elapsed time for SP1

986

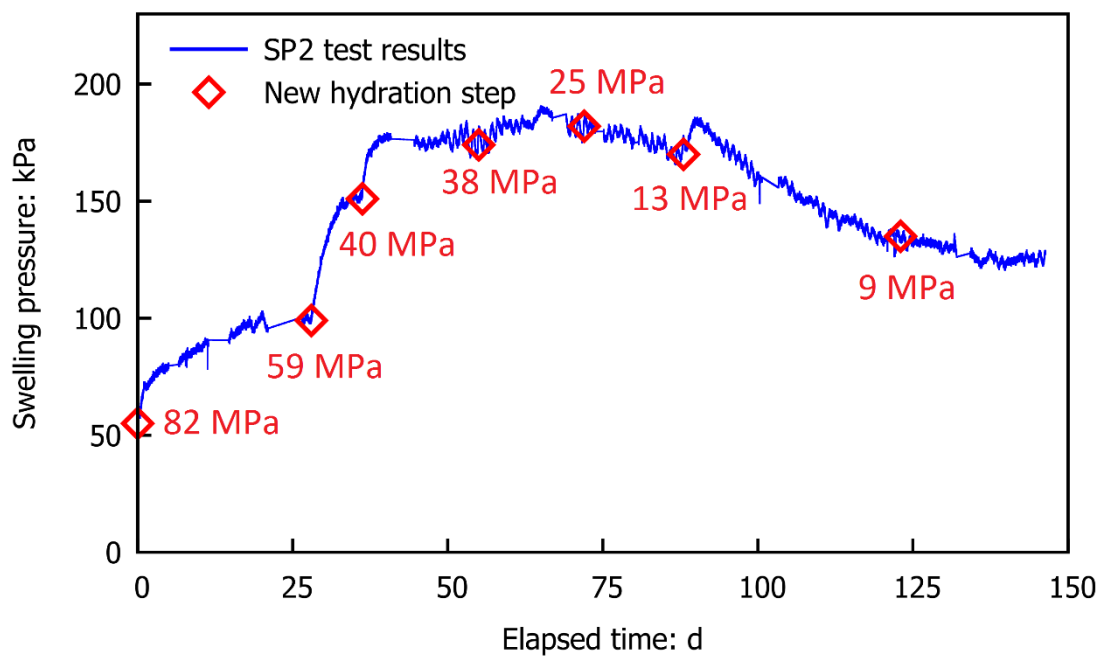


987

988

989 **Fig. 8b** Swelling pressure as a function of elapsed time for SP2

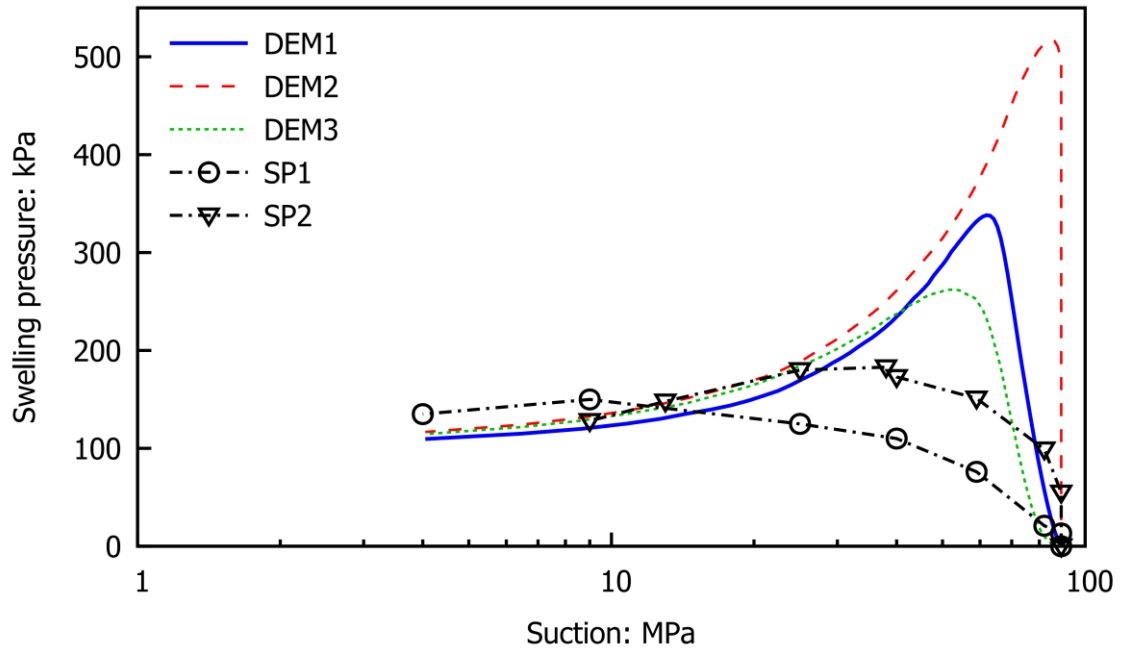
990



991

992 **Fig. 9** Swelling pressure as a function of decreasing suction for SP1 and SP2, along with the
993 mean value obtained for DEM1, DEM2 and DEM3 simulations.

994



995

996

997

998

999
1000
1001

Fig. 10a Picture of the SP1 sample after dismantling at 4 MPa of suction. The cell diameter is 60 mm



1002
1003

1004
1005
1006

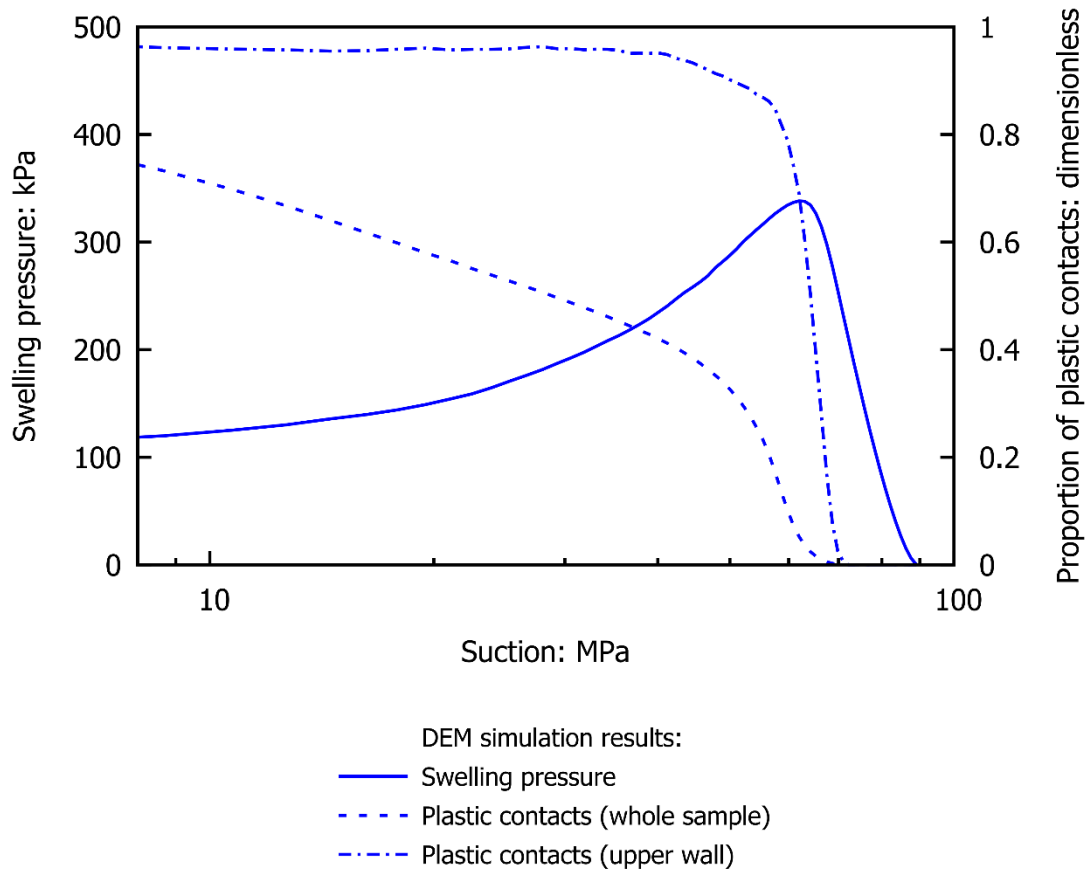
Fig. 10b Picture of the SP2 sample after dismantling at 9 MPa of suction. The cell diameter is 60 mm



1007
1008
1009
1010

1011 **Fig. 11a** Mean value of swelling pressure, proportion of plastic contacts in the sample and
1012 proportion of plastic contacts at the top wall in DEM1

1013

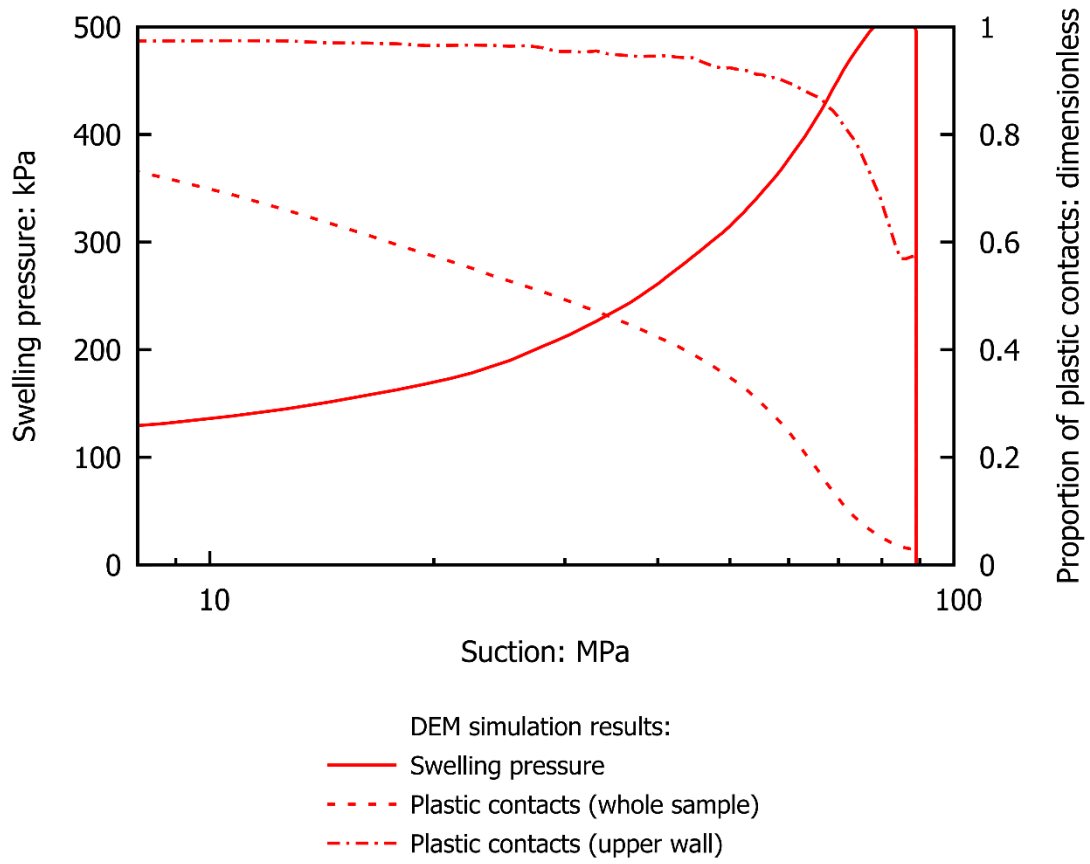


1014

1015

1016

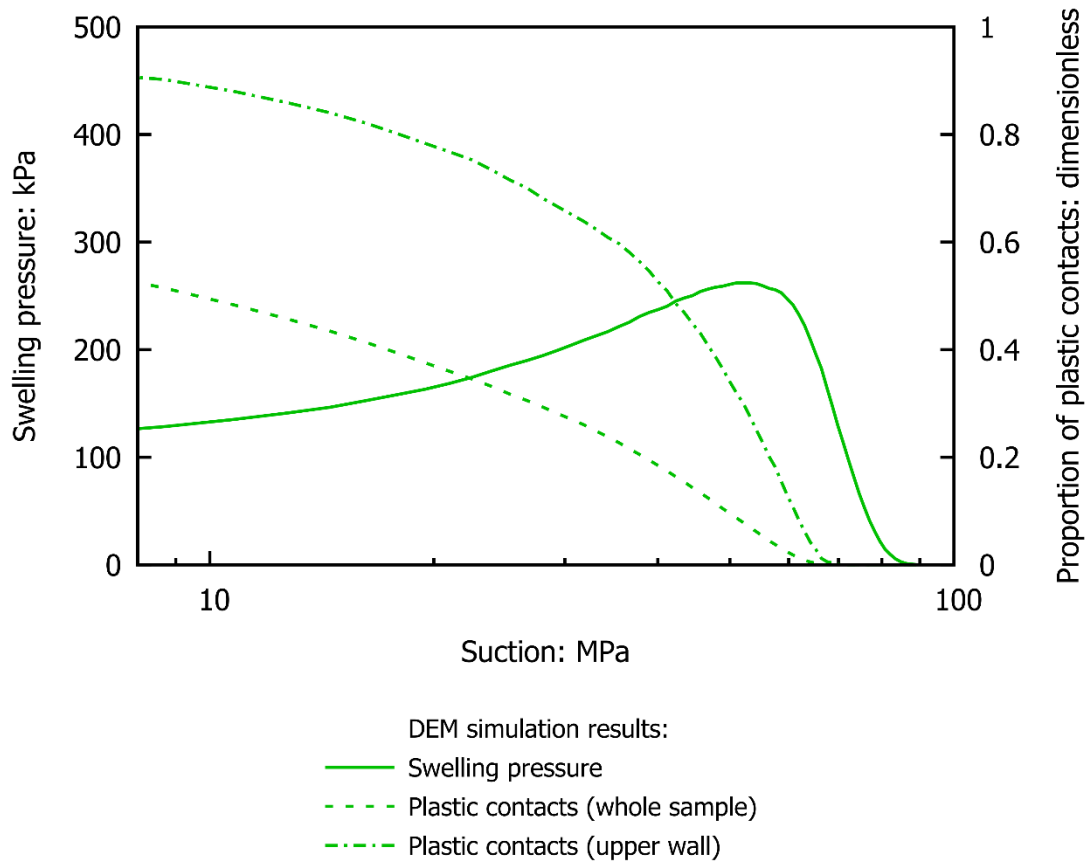
1017 **Fig. 11b** Mean value of swelling pressure, proportion of plastic contacts in the sample and
1018 proportion of plastic contacts at the top wall in DEM2
1019



1020
1021
1022

1023 **Fig. 11c** Mean value of swelling pressure, proportion of plastic contacts in the sample and
1024 proportion of plastic contacts at the top wall in DEM3

1025

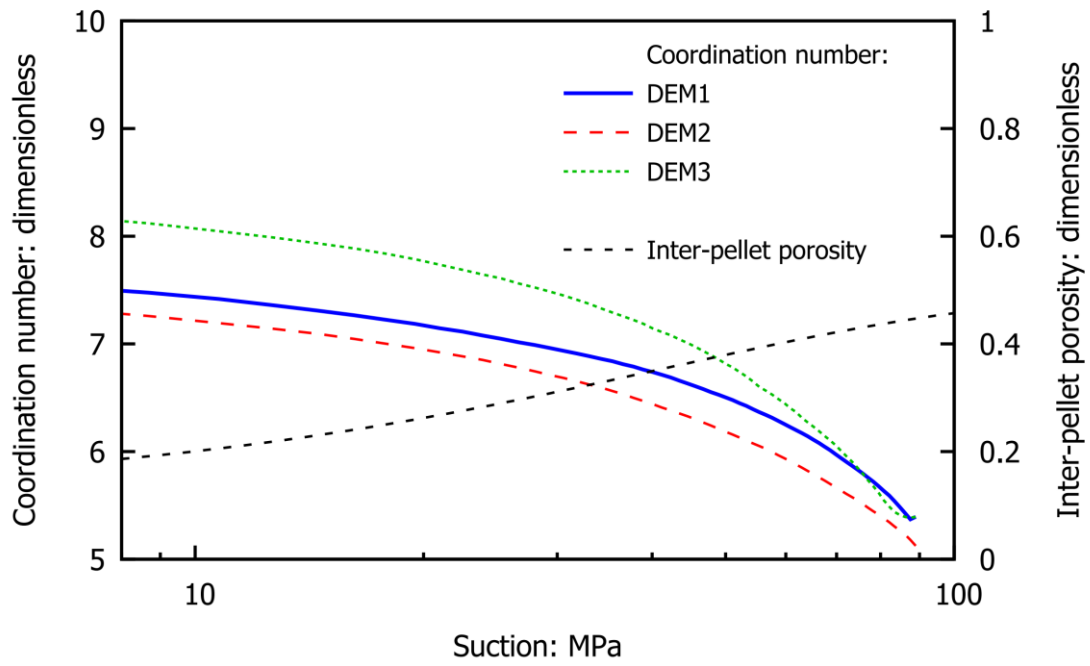


1026

1027

1028

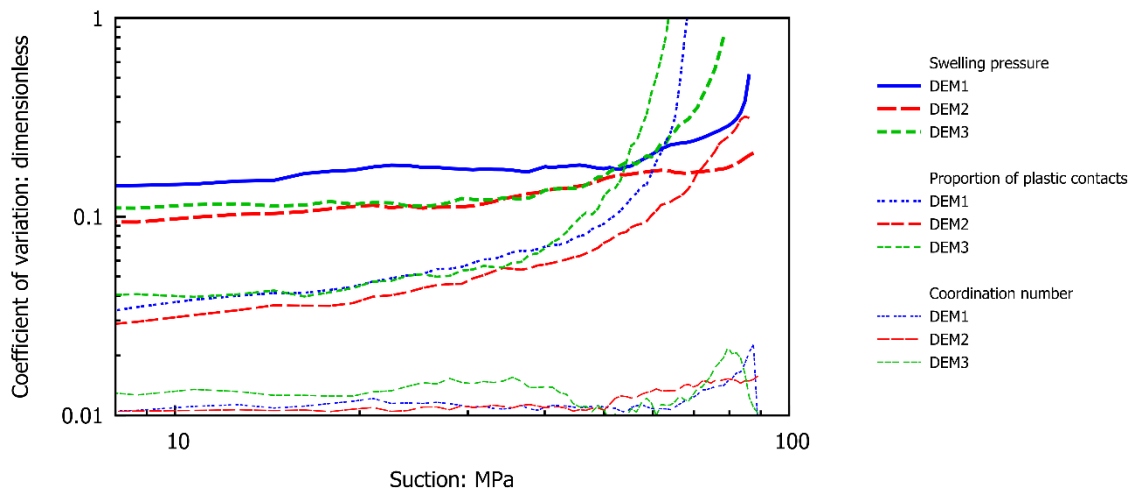
1029 **Fig. 12** Coordination number in DEM1, DEM2 and DEM3 simulations (mean values) and
1030 evolution of inter-pellet porosity upon suction decrease (identical in all DEM simulations).
1031



1032
1033
1034
1035

1036 **Fig. 13** Coefficient of variation of swelling pressure, proportion of plastic contacts and
1037 coordination number in DEM1, DEM2 and DEM3 simulations

1038

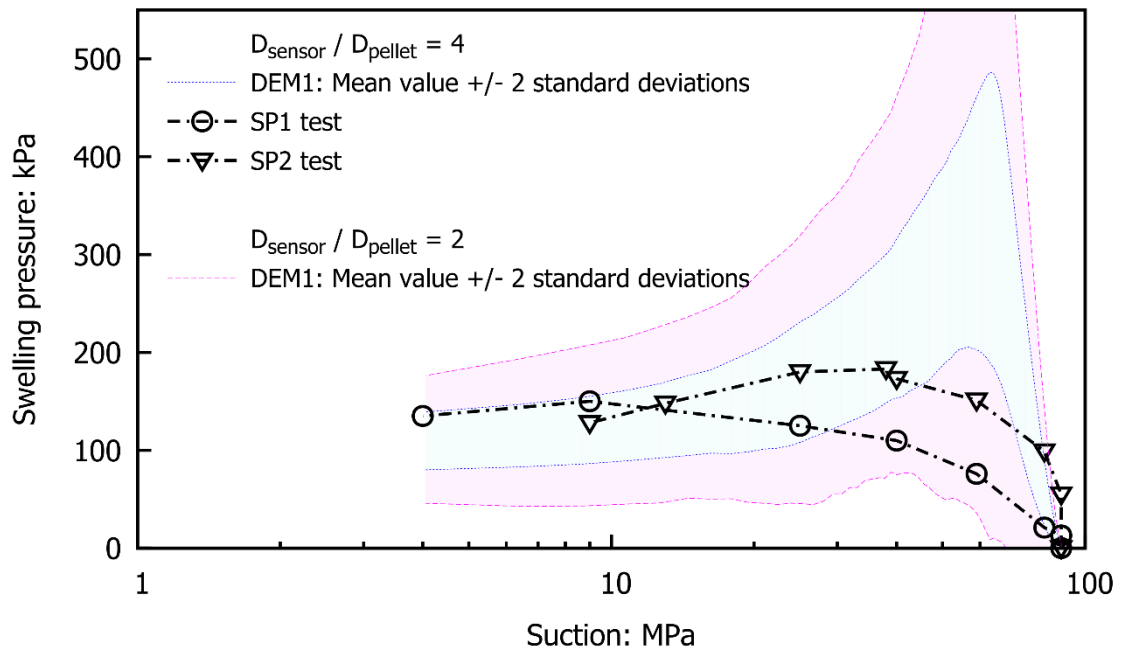


1039

1040

1041

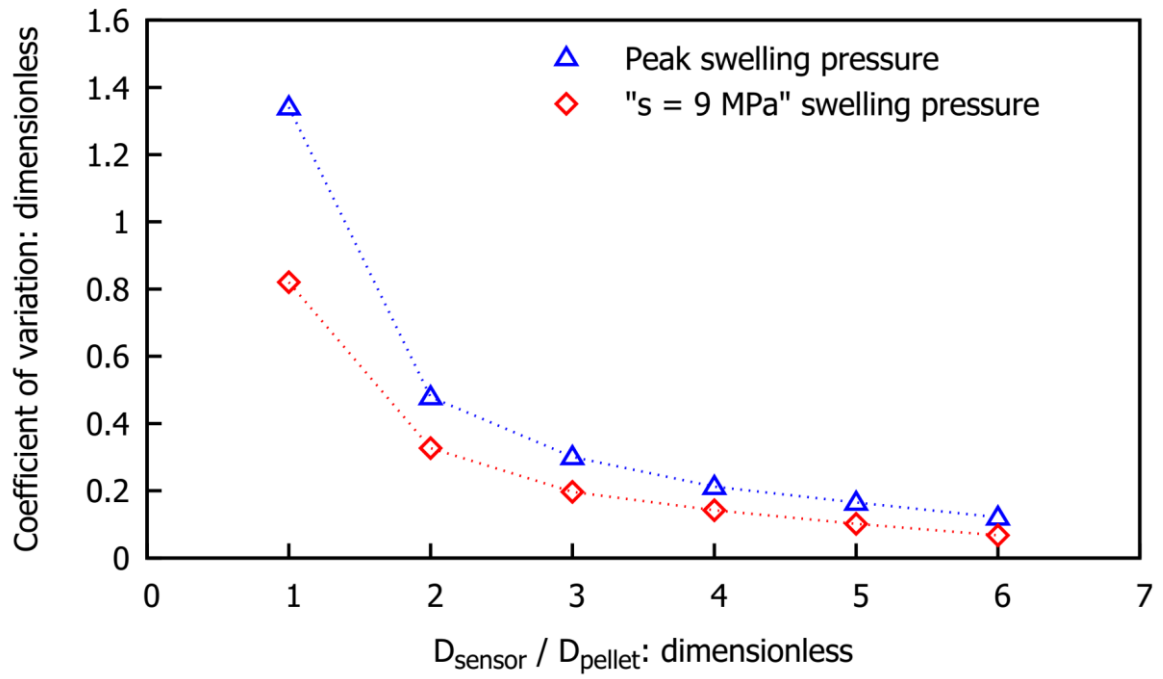
1042 **Fig. 14** Variability of the measured swelling pressure in DEM1 simulations for two sensor sizes
1043



1044
1045
1046
1047

1048 **Fig. 15** Coefficient of variation of the measured swelling pressure in DEM1 simulations at peak
1049 and at 9 MPa of suction

1050



1051

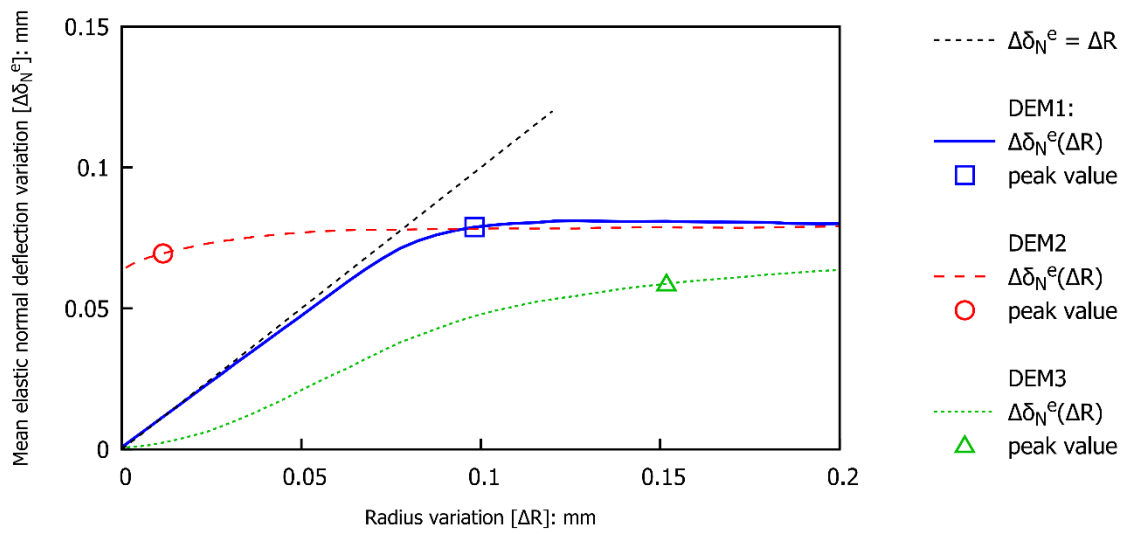
1052

1053

1054

1055 **Fig. 16** Evolution of the mean elastic normal deflection in the numerical sample in DEM1, DEM2
 1056 and DEM3 simulations. Mean values are plotted

1057



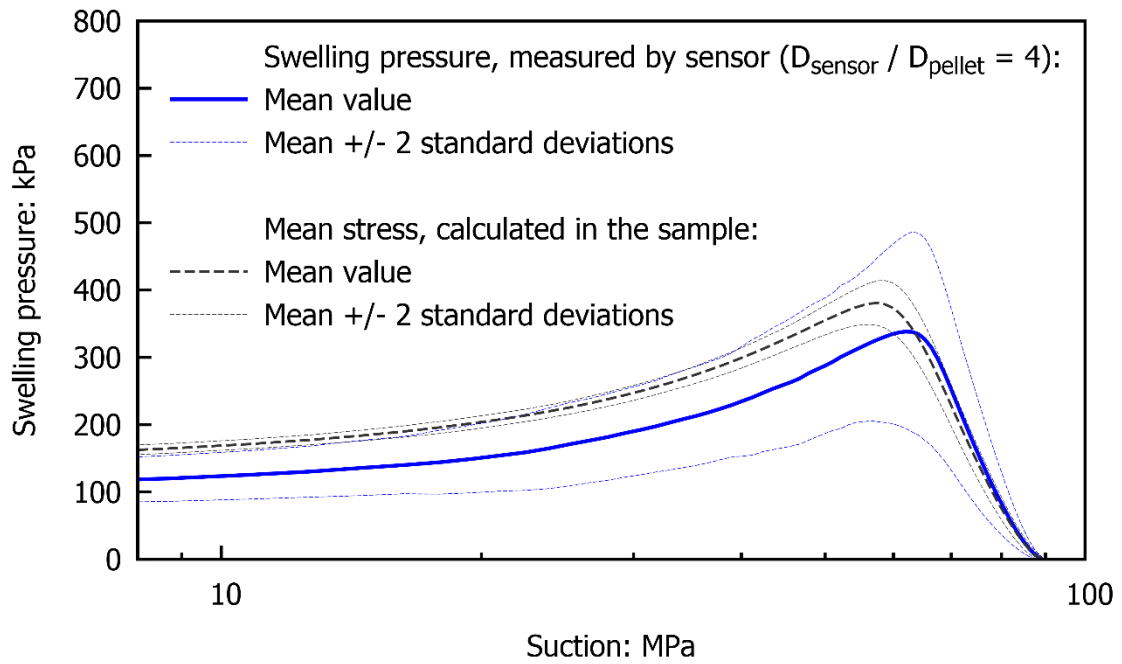
1058

1059

1060

1061 **Fig. 17** Comparison of the mean stress calculated in the sample and the swelling pressure
1062 measured by the sensor as functions of decreasing suction for DEM1 simulations

1063



1064

1065

1066